Published in
Encyclopedia of Analytical Chemistry, 1-29, 2011
which should be used for any reference to this work

Diode Laser Spectroscopic Monitoring of Trace Gases

Stephane Schilt
Time and Frequency Laboratory, University of Neuchâtel, CH-2000 Neuchâtel, Switzerland

Frank K. Tittel
Rice University, Houston, USA

Konstantin P. Petrov
Gemfire Corporation, Palo Alto, USA

Modern diode laser spectroscopy is becoming an important and a more widely used tool for detection and measurement of trace gases. The change is driven by the recent advances in diode laser technology and diode laser frequency conversion techniques, which now push the limits of emission wavelength, output power, operating temperature, miniaturization, and cost. Basic features of the diode laser now find new, interesting, and unique use in well-established laboratory and field applications related to trace-gas detection and, in some instances, even transform the traditional spectroscopic methods. It is the purpose of this chapter to familiarize the reader with the key elements of diode laser technology and analytical methods used in diode laser spectroscopy.

1 INTRODUCTION

Sensors based on tunable diode lasers have found widespread applications in the sensitive and selective detection of environmentally important atmospheric trace gases in real time. The motivation for such precise species concentration measurements of gaseous compounds in ambient air includes diverse fields such as urban (e.g. automobile traffic, air quality in large enclosed structures), industrial (e.g. fence line perimeter monitoring in the petrochemical industry, combustion sites, and waste incinerators), rural (e.g. horticultural greenhouses, rice agroecosystems) emission studies; chemical analysis and control of manufacturing processes (e.g. HF, NH_3, and HCl in semiconductor fabrication facilities and HF in aluminum smelters); biomedical sensing of physiologically important molecules (e.g. NO and CO); atmospheric chemistry (e.g. CO, CO_2, CH_4, and H_2CO in global studies of the environment); and spacecraft habitat air-quality monitoring.[1,2]

Numerous analytical instruments based on optical and nonoptical techniques have been developed in the past. In general, these instruments have some, but not all, of the desired characteristics including high sensitivity, selectivity, multicomponent detection capability, room-temperature operation, large dynamic range, automatic operation, small size, high reliability, ease of use, and cost-effectiveness in terms of initial and maintenance

costs. An ideal gas sensor technology that meets all these diverse requirements is, however, a challenging research and development task. Today's state-of-the-art laser spectroscopy, for example, is not far from being able to meet these requirements, and recent significant technological advances may further change the way it is used in future applications. Areas of technology that have seen a particularly strong improvement are tunable diode lasers, both near-infrared (NIR) and mid-infrared (MIR); novel nonlinear materials for optical frequency conversion; optical fiber and semiconductor amplifiers; low-noise, room-temperature detectors; and advanced data acquisition and signal processing techniques.

Such new diode-laser-based spectroscopic sensors are beginning to provide excellent sensitivity and selectivity to an increasing number of organic and inorganic gaseous compounds in the infrared spectral region. This region consists of both the NIR (0.8–2 μm), which can be accessed by an increasing number of distributed feedback (DFB) telecommunications diode lasers or vertical-cavity surface-emitting lasers (VCSELs), and the MIR (2–20 μm), which can be accessed by lead-salt and antimony-based diode lasers, quantum cascade lasers, and compact sources based on difference-frequency mixing of commercially available diode and fiber lasers. Performance characteristics of several recent optical architectures of MIR gas sensors that have been developed and applied to real-world spectroscopic applications in the field and laboratory are discussed. An effective method to increase sensitivity is to increase the effective optical path. This is possible for *in situ* open-path atmospheric measurements, but numerous applications require a compact extractive technique based on multipass cells (White, Herriott designs).

The NIR region is characterized by the presence of the first- and higher-order overtone and combination bands for many important gases. However, the transition strengths of the fundamental vibrational bands in the MIR are at least one to two orders of magnitude stronger, making this spectral regime the region of choice for high-sensitivity laser absorption spectroscopy. The detection sensitivity of current diode-laser-based gas sensors using direct absorption spectroscopy is limited by etalon fringes and laser feedback noise to 10^{-5} to 10^{-6} relative absorption. Etalon fringes are optical interferences arising between the main laser beam and small parasitic reflections originating from various parallel optical surfaces in the beam path (windows, lenses, etc.), and they act as low-finesse Fabry–Perot cavities. Optical fringes limit the precision of spectroscopic sensors by creating time-dependent background structures that superimpose the analyzed gas absorption signal. Even with a careful optical alignment and use of antireflective coated surfaces, it is very challenging to reduce etalon fringes below 10^{-6} fractional absorption. Multipass cells are particularly affected by etalon fringes because of the optical interferences between adjacent focal spots on the cell mirrors.[3] Different hardware and software efforts have been made to reduce the impact of etalon fringes. Hardware modulation approaches have been implemented to average out fringes by applying either a mechanical modulation to the optical path length through the vibration of an optical element[4] or a low-amplitude modulation (dither) to the laser current.[5] Software methods apply digital postdetection filtering to suppress fringes.[6] However, all these methods are more efficient when the fringes period is much smaller than the width of the analyzed absorption line and the most difficult etalons to deal with remain those whose free spectral range is comparable to the absorption linewidth, as it is not possible to reduce these fringes without affecting the absorption signal. The major impact of etalon fringes on a spectroscopic gas sensor results from temperature fluctuations over time, which causes the interference fringes to slowly drift in wavelength such that they cannot be removed by a zero baseline subtraction technique. This results most often in an undesirable fluctuation of the sensor response with respect to temperature changes. A detailed analysis of the origin and impact of optical fringes in a spectroscopic gas sensor can be found in a recent paper by Werle.[7]

In addition to direct absorption spectroscopy, various techniques such as wavelength modulation spectroscopy (WMS), frequency modulation spectroscopy (FMS) or two-tone frequency modulation spectroscopy (TTFMS), balanced homodyne or balanced ratiometric detection (BRD), optoacoustic spectroscopy (OAS), and cavity ring-down spectroscopy (CRDS) can be utilized. Of these, only OAS and CRDS offer a means for avoiding the baseline variations caused by etalon fringes, which often limit sensitivity as previously discussed.

2 FUNDAMENTALS OF GAS-PHASE SPECTROSCOPY

2.1 Atmospheric Trace Gases

Spectroscopic trace-gas detection is a method allowing one to compute the concentration of a known gas, or gases, from a measured optical absorption spectrum of the gas mixture (in practice, a small fragment of the spectrum may be measured). The procedure requires a good quantitative knowledge of the gas absorption characteristics. This knowledge is the realm of molecular spectroscopy, a complex and highly developed subject that is outside the scope of this chapter. A few fundamental spectroscopic concepts and formulae that

are directly applicable to gas detection are, however, summarized in this section.

Each atom or molecule, small or large, is uniquely characterized by a set of energy levels. Transitions between levels by absorption or emission of electromagnetic radiation result in highly specific spectroscopic features. These features allow both the identification and quantification of the molecular species, such as atmospheric trace gases. Molecules may undergo transition between electronic, vibrational, and rotational states when exposed to electromagnetic radiation, resulting in absorption spectra. These spectra consist of a number of discrete absorption lines. Each line has a certain linewidth and shape that depend on temperature and the surrounding environment, so the lines may form resolved or unresolved bands (Figure 1); some will be intense, while others will be weak. Transitions between molecular rotational–vibrational (ro-vibrational) states occur in the infrared 'fingerprint' region of the electromagnetic spectrum, approximately between the wavelengths of 2.5 and 25 μm. Often also overtone and combination-overtone ro-vibrational bands are possible with significantly lower line intensity as compared to those for fundamental vibrational bands, and the corresponding wavelengths are in the 0.8 to 2.5 μm spectral region. Transitions between electronic states of atoms and molecules occur in the ultraviolet and visible spectral region, 200–500 nm.

All polyatomic molecules, with the exception of homonuclear diatomic molecules (e.g. N_2), absorb infrared radiation. The absorption changes the state of molecular rotation and vibration. An absorption spectrum, therefore, depends on the physical properties of the molecule, such as size and shape, and hence, each molecule is characterized by a unique spectral 'signature'. Spectra of linear and some nonlinear polyatomic molecules consist of an array of individual or small groups of lines. In the case of large polyatomic molecules (e.g. benzene, C_6H_6) at atmospheric pressure, there are many lines overlapping each other, resulting in broad spectral features with some occasional peaks. These features occur in the majority of spectra and are the principal reason for the sensitivity and selectivity of trace-gas detection in the infrared region.

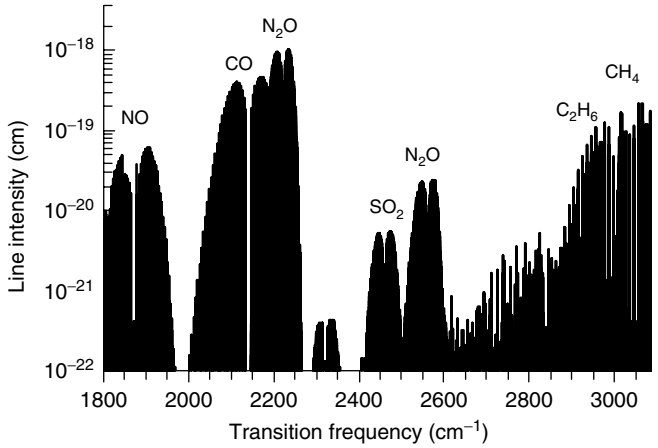

Figure 1 Survey absorption spectra of several atmospheric trace gases in the 3.1- to 5.6-μm wavelength region (3200–1800 cm^{-1}).[8,9]

There are numerous atmospheric trace gases (Table 1). Their concentrations would normally be in the parts per billion (ppb, 10^{-9}) to parts per million (ppm, 10^{-6}) range. Minimum and maximum concentrations range from parts per trillion (ppt, 10^{-12}) to percentage (%, 10^{-2}). There is much spectroscopic data available in the literature[1,2] and electronic form, which are important tools in the identification and development of specific detection strategies, especially in the presence of interfering species.[8–10]

2.2 Absorption Lineshape

In the absence of optical saturation and particulate-related scattering, the intensity of light $I(x)$ propagating in a homogeneous gas follows the Beer–Lambert law (Equation 1):

$$I(x) = I_0 \exp(-\sigma_m(\nu) N_m x) \tag{1}$$

Table 1 Analysis of atmospheric gas traces.

Molecule	Absorption line (mm)	Overtone MDC (ppm m)	Fundamental MDC (ppm m)
CO_2	4.23	8[11]	0.0072
OCS	4.85	NA	0.023
N_2O	4.54	220[11]	0.036
	2.87	–	1.3
CO	4.6	100[12]	0.044
HCl	3.5	1.3[13]	0.050
HCN	3.0	0.29[14]	0.081
C_2H_6	3.34	NA	0.081
HF	2.4	0.2[15]	0.090
C_2H_2	3.08	0.08[14]	0.1
CH_4	3.3	15[13]	0.23
HBr	3.81	0.6[14]	0.32
H_2CO	3.6	50[14]	0.54
NO_2	3.46	0.5[16]	1.8
NH_3	2.94	2[17]	2.7
NO	5.3	60[14]	4
O_3	4.75	NA	9
SO_2	4.0	NA	40
H_2S	3.72	0.2[15]	54
H_2O	3.3	NA	NA

MDC, minimal detectable concentration.
Values computed for the following parameters: (i) fundamental, $p = 100$ torr; $T = 298$ K; MDC $= 2 \times 10^{-4}$ using direct absorption and (ii) overtone, MDC $= 1 \times 10^{-5}$ using either balanced detection/FM techniques.

Here, m is the gas species index that labels the molecular density N_m and absorption cross section $\sigma_m(\nu)$. The molecular absorption cross section depends on frequency and has the units of square centimeter per molecule (cm^2/mol). It is the sum of cross sections of all individual ro-vibrational transitions (Equation 2):

$$\sigma_m(\nu) = \sum_n S_n \Gamma(\nu - \nu_n) \tag{2}$$

We label the transitions using the index n; thus ν_n is the frequency of the n-th transition and S_n is its intensity (also referred to as the line strength, usually expressed in units of cm^{-1}/(molecule cm^{-2}) when the frequency is expressed in inverse centimeter). Technically, both these quantities should also bear the index m to remind that they refer to a certain gas species, but for simplicity, it is not done here.

The function $\Gamma(\nu)$ describes the lineshape and has the same analytical form for all transitions. In MIR spectroscopy, the broadening of an individual transition due to finite upper-level lifetime (leading to the natural linewidth) is insignificant compared to the broadening by the other two important mechanisms – thermal motion and molecular collisions. Their individual and combined effects on a molecular transition at a frequency ν_n are expressed as follows (Equations 3–7):

Thermal motion (Gaussian):

$$\Gamma(\nu) = \frac{1}{\Delta\nu_T\sqrt{\pi}} \exp\left[-\left(\frac{\nu}{\Delta\nu_T}\right)^2\right] \tag{3}$$

$$\Delta\nu_T = \frac{\nu_n}{c}\sqrt{\frac{2kT}{M}} \tag{4}$$

Molecular collisions (Lorentzian):

$$\Gamma(\nu) = \frac{1}{\pi\gamma_n P}\left[1 + \left(\frac{\nu}{\gamma_n P}\right)^2\right]^{-1} \tag{5}$$

Combined broadening (Voigt):

$$\Gamma(\nu) = \frac{1}{\gamma_n P} V\left(\frac{\nu}{\gamma_n P}; \frac{\Delta\nu_T}{\gamma_n P}\right) \tag{6}$$

$$V(x, y) = \frac{1}{\pi\sqrt{\pi}} \int_{-\infty}^{+\infty} \frac{\exp(-t^2)}{1 + (x + yt)^2} \mathrm{d}t \tag{7}$$

Here c is the speed of light in vacuum; k, the Boltzmann constant; T, the gas temperature; M, the mass of the molecule; P, the total gas pressure, and γ_n, the coefficient of pressure broadening (it should be noticed that the pressure-broadening coefficient γ_n is gas-mixture dependent, as collision broadening varies with respect to the surrounding colliding molecules). The quantities $\Delta\nu_T$ and $2\gamma_n P$ are referred to as the Doppler- and pressure-broadened linewidths ($2\gamma_n P$ is the full width at half maximum of the Lorentzian lineshape, $\Delta\nu_T$ is the half width at $1/e$ of the Gaussian lineshape). The lineshape that results from the combined effect of Doppler and pressure broadening is a convolution of the two respective lineshapes. It is known as the Voigt profile, and its mathematical expression $V(x, y)$ cannot be further simplified. The physical significance of the convolution is that the Voigt profile has different asymptotic shapes for very low and very high gas pressures. At low pressure, molecular collisions are less frequent, leaving thermal motion the dominant broadening mechanism – the corresponding lineshape is near-Gaussian. As the gas pressure increases, the collisions take over, and the resulting lineshape is near-Lorentzian (Figure 2).

The previous expressions do not include the effect of pressure shift, which is typically in the range of several megahertz per atmosphere. The shift is very small compared to the width of an atmospheric-pressure-broadened line, typically several gigahertz.

It is common practice in infrared spectroscopy to express transition frequencies in inverse centimeters (cm^{-1}), or wavenumbers, defined simply as the inverse of the transition wavelength in vacuum, $\nu = \lambda^{-1}$. Multiplying this quantity by c gives the frequency in Hertz;

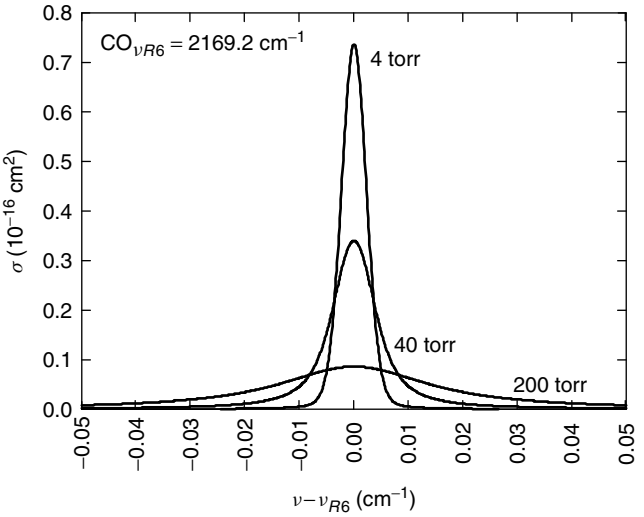

Figure 2 Frequency-dependent absorption cross-section of the R(6) fundamental transition of carbon monoxide at room temperature, plotted for different values of background air pressure. The horizontal axis is in cm^{-1} relative to the line center, $\nu_{R6} = 2169.2\,cm^{-1}$. Area under each curve, or line intensity, is the same: $S = 4.44 \times 10^{-19}$ cm. At 40-torr background air pressure, the Doppler- and collision-broadened linewidths are approximately equal to $0.003\,cm^{-1}$.

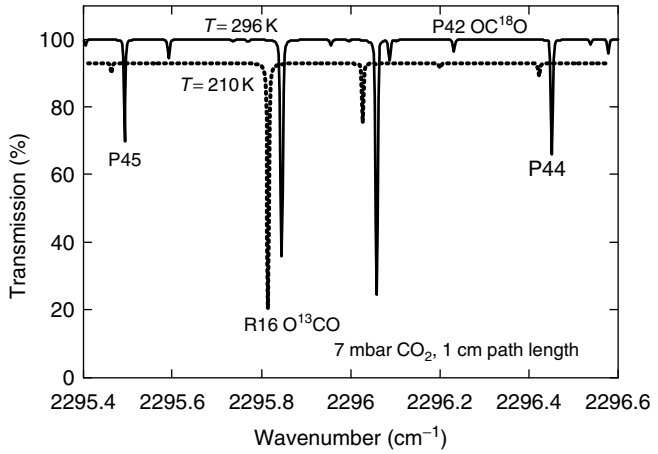

Figure 3 Absorption spectra of pure CO_2 at a pressure of 7 mbar over a 1-cm path calculated at two different temperatures using the HITRAN database.[9] The dotted trace has been offset for clarity and corresponds to $T = 210$ K, simulating the surface atmosphere of Mars. The strong dependence of line intensity on temperature for the transitions P44 and P45 should be noted.

thus, $1\,\text{cm}^{-1}$ is roughly 30 GHz. We shall use both units throughout this chapter, where appropriate.

One can verify, by integrating the absorption cross section of an individual transition over frequency, that it is independent of the broadening mechanism and is equal to the line intensity S_n, in the units of centimeter per molecule. Line intensity is proportional to the lower-state population density of a transition and thus depends on temperature (Figure 3). To a good approximation, especially at low temperatures, the sum of line intensities of all transitions in a band is independent of temperature and is known as the band strength B_m (Equation 8).

$$B_m = \int_{-\infty}^{+\infty} \sigma_m(\nu)\,\mathrm{d}\nu = \sum_n S_n \tag{8}$$

It contains information on the vibrational electric dipole moment.[8] Thus, in order to compute the absorption cross section $\sigma_m(\nu)$ at any frequency, one must know the values ν_n, S_n, and γ_n for all transitions. These parameters have been measured and calculated for many lightweight gas molecules across the microwave and infrared spectra and compiled into extensive databases such as HITRAN[9] and GEISA.[10] Numerically accurate absorption spectra can be computed based on these data not only for single gas species but also for gas mixtures.

2.3 Spectra of Multicomponent Gas Mixtures

Analytical formulae given in the preceding section apply also to gas mixtures. The total absorption cross section $\sigma(\nu)$ is then a weighted average of absorption cross sections of individual species, with the mole fraction C_m of each species used as the weight coefficient (Equations 9 and 10):

$$\sigma(\nu) = \sum_m C_m \sigma_m(\nu) \tag{9}$$

$$\sum_m C_m = 1 \tag{10}$$

For each of the m species, the pressure-broadening coefficients γ_n generally depend on the transition. They also depend on the type of molecule with which the collisions occur. In general, partial pressures (P_m) in conjunction with the appropriate pressure-broadening coefficients (γ_{nm}) should be used to compute the overall pressure broadening from all gases present in the background (this includes self-broadening) (Equation 11).

$$\gamma_n = \sum_m P_m \gamma_{nm} \tag{11}$$

Air-broadening coefficients are particularly useful in calculations and are listed in spectroscopic databases.[9,10]

In trace-gas sensing applications, however, the species of interest are often present in very low concentrations, so that self-broadening and broadening against other trace gases can be neglected in calculations, and air-broadening alone will suffice. For the conditions of atmospheric pressure broadening, $\gamma P \gg \Delta\nu_T$, the Doppler contribution to the overall linewidth can often be neglected, and the lineshape can be treated as pure Lorentzian. Likewise, at pressures low enough to ensure $\gamma P \ll \Delta\nu_T$, the lineshape can be treated as pure Gaussian. In either case, calculation of the line profile is simplified considerably.

At intermediate total pressures, $\gamma P \sim \Delta\nu_T$, which for most lightweight gases range from 5–100 torr, calculation of the Voigt profile is necessary to obtain numerically accurate absorption spectra. Methods for approximate calculation of the Voigt profile, and the related plasma dispersion function, are now a well-developed subject. We have found the approximations published by Humlicek[18] to be particularly useful.

3 LASER SPECTROSCOPIC SOURCES

3.1 Advantages of Diode Lasers

Soon after the first semiconductor (diode) laser was developed in 1962, diode laser spectroscopy became a firmly entrenched technique for detection, identification, and measurement of molecular and atomic species in the gas phase. The reason for its wide acceptance in

Table 2 Performance characteristics of room-temperature single-frequency NIR diode lasers (DFB type).

Parameter	Unit	Typical values
Center wavelength	nm	670, 780, 810, 860, 980, 1060, 1310, 1550
Gain bandwidth	nm	20–50
Output power	mW	3–200
Mode size	mm	1×3
Linewidth	MHz	10–300
Tuning response	nm K^{-1}	0.1–0.3
Tuning response	GHz mA^{-1}	0.3–2
Threshold current	mA	20–90
Modulation bandwidth	GHz	2–40

the scientific community was twofold. First, narrow-linewidth light sources such as lasers were well suited for probing the inherently narrow molecular and atomic transitions, so that both the lineshape and line intensity could be measured accurately and rapidly. Lasers simply offered better wavelength resolution (linewidth) and spectral brightness (power emitted per unit linewidth) than conventional grating or prism monochromators. Second, among all lasers, diode lasers offered a unique combination of tunability, output power, small size, and modulation capabilities (Table 2). In other words, they are significantly more convenient to use than other sources. Perhaps, the most important advantages of diode lasers are the simple excitation in the form of electric current and the fact that the laser wavelength and output power depend on the current. For small changes in the injection current, that dependence is nearly *linear* and *instantaneous*, allowing predictable and fast wavelength control. This advantage is discussed in Section 4.3. DFB lasers can be current-tuned at a typical rate of 1 GHz mA^{-1}. VCSELs constitute another type of semiconductor lasers that has rapidly developed in the past two decades, originating from the optical telecommunications industry. Owing to their surface-emitting property (in contrast to edge-emitting DFB lasers) and their associated on-wafer testing capabilities, these lasers offer a high potential for low-cost mass production. Despite their lower optical power (compared to DFB lasers) in the milliwatt or submilliwatt range, VCSELs are attractive laser sources for compact gas sensors because of their very low electrical power consumption and large tunability (the current-tuning is one to two orders of magnitude larger than that in a DFB laser, at the level of 30–150 GHz mA^{-1}[19]).

Diode laser spectroscopy is divided into two categories according to the spectral region used. MIR spectroscopy is used in the 'fingerprint' region from 2.5 to 25 μm where most molecular species exhibit fundamental absorption. It offers the highest detection sensitivity among spectroscopic methods, primarily because the fundamental absorption bands are very strong. Diode lasers operating at MIR wavelengths typically deliver 100-μW output power and require cryogenic cooling (more on this in Section 3.3). Quantum cascade lasers constitute a more recent technology for single-mode MIR light generation with higher optical power and room-temperature operation capabilities (most often in pulsed mode). For these reasons, they have become the most appropriate laser sources for MIR spectroscopy for one decade. NIR, or 'overtone', spectroscopy employs room-temperature diode lasers (DFB or VCSEL) at wavelengths below 2 μm. Detected here are the short-wavelength molecular overtone transitions that are typically a factor of 30–300 weaker than the fundamental transitions. These two types of molecular spectroscopy represent the two different choices made in the trade-off between absorption strength and the optical power available to detect it. MIR spectroscopy is used whenever higher sensitivity is needed, but at the expense of higher cost and cryogenic cooling in some cases (for the laser and/or detector). Overtone spectroscopy is the method of choice in applications where lower sensitivity can be tolerated but where low cost, reliability, and room-temperature operation are paramount. Alternative techniques for the generation of MIR light for spectroscopic applications are discussed in Section 3.4.

3.2 Overtone Band Detection with Near-infrared Diode Lasers

NIR spectrometers usually employ commercial diode lasers with emission wavelengths from 780 to 2400 nm. Gas detection at these wavelengths is based on the molecular vibration overtone and combination-overtone bands that are significantly less intense than the fundamental bands. For example, the lines of the first overtone stretch vibration band of methane centered at 1.6 μm are roughly 160 times weaker than those of the fundamental band. Thus, ambient methane would cause a 0.005% absorption over a 1-m path length at this wavelength at room temperature.[9] Reliable measurement of such low absorption is difficult even under laboratory conditions, so longer path lengths or special measurement techniques are necessary to render a satisfactory signal-to-noise ratio for applications requiring trace-level monitoring.

Overtone spectrometers usually have plenty of optical probe power to deal with this problem. NIR diode lasers emit anywhere from 1 to 100 mW of single-frequency radiation with low excess noise 15 – 35 dB over shot-noise limit is typical – and it can be detected with a silicon photodiode[20] at wavelengths shorter than 1 μm and with indium-gallium-arsenide (InGaAs) photodiodes

up to 1.65 μm (2.6 μm for extended InGaAs). They are fast, with modulation bandwidths of over a gigahertz allowing rapid scanning and fast frequency modulation (FM), leading to gas detection in real time.

High output power levels have two important benefits. First, detector noise can be neglected and the measurement of absorption be performed near the optical shot-noise limit. For example, Allen et al.[16] report a detection sensitivity of $2 \times 10^{-7}\,\mathrm{Hz}^{-1/2}$ absorption units with the use of a 1.3-μm diode laser and a balanced ratiometric detector. Second, with high initial power available in a beam, one can employ a multipass cell to propagate the beam back and forth through a gas sample, achieving long effective path lengths and thus increasing the observed absorption signal. Although the throughput of such a cell decreases exponentially as the number of passes increases (also see Section 4.1), there is still plenty of light left at the end to permit measurements that are not limited by detector noise.

NIR overtone spectrometers, such as one developed by Uehara and Tai,[21] are usually built to detect one or a few specific gases, for two reasons. First, the NIR wavelength region from 780 to 2400 nm is not covered completely; diode lasers are available at only few discrete wavelengths, and each has a limited tuning range of a few nanometers when operated without an external cavity. Second, these devices are relatively inexpensive, making it economical to have several dedicated lasers, each detecting one gas species, in a single instrument. This configuration is also attractive because different gas species can be measured in parallel. For example, several groups have developed a gas sensor that can do this using one common beam path through the sample and one detector.[22]

Owing to their large and fast tuning capability (from several tens to hundreds of gigahertz tuning at megahertz rate[23]), VCSELs enable to simultaneously detect two or more species in a single current scan.[24] Initially developed at telecom wavelengths, VCSELs have then been extended to both shorter and longer wavelengths and nowadays cover the range 0.7–2.3 μm. Many simple molecules with resolved absorption lines have been addressed by VCSELs, including O_2,[25–27] H_2O,[28] NH_3,[29] CH_4,[23,24] HCl,[24,30] and CO,[31] as well as larger molecules with partially unresolved spectra, e.g. C_2H_4O.[32] Another favorable property of VCSELs over DFBs is their low beam divergence and circularly symmetric output. As a consequence, very simple sensor geometries have been designed based on VCSELs, involving a minimum number of optical elements. In the simplest scheme, a VCSEL and a photodiode are mounted side-by-side at one edge of a compact gas chamber, and a spherical mirror, mounted at the other edge, focuses the laser light on the detector after a double-pass interaction length of typically 20 cm.[27] Such a simple architecture with a short path length does not aim at achieving an extreme sensitivity, but simplicity, reliability, lightweight, and ruggedness are key requirements for compact, low power consumption, and potentially low-cost gas sensors for large-scale applications and VCSEL are especially well suited in this context.

Combining a bottom half-VCSEL with a top microelectromechanical systems (MEMS) movable Bragg-mirror membrane results in a broadly tunable laser in a very compact device (Figure 4). In addition to the main advantages of VCSELs (inherent longitudinal single-mode behavior, compactness, low power consumption, etc.), a large tunability is provided by the electrothermal or electrostatic actuation of the membrane, which acts as a movable external mirror. With more than 60-nm continuous static tuning range demonstrated in the optical telecommunication C-band[33] with a 3-dB tuning bandwidth of 180 Hz[34] and all the necessary properties for the implementation of modulation spectroscopy techniques,[35] these so-called MEMS-VCSELs constitute an attractive technology for multigas sensing using a single laser source. Even if they are not yet commercialized, laboratory-prototypes have demonstrated a nice potential for gas spectroscopy,[33,34] and the operation range of these devices is currently pushed toward shorter and longer wavelengths.

Alternatively, a single external-cavity diode laser (ECDL) with a large tuning range can be used. In

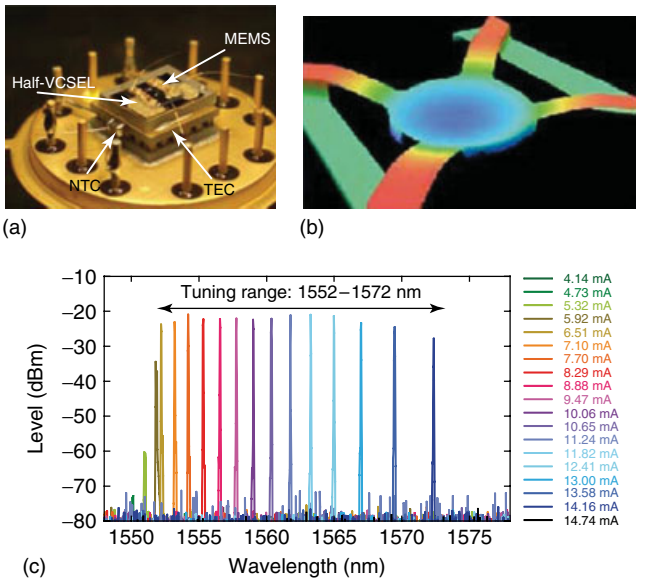

Figure 4 (a) Assembly of an MEMS-VCSEL[35] into a T08-package with an active temperature control. (b) Confocal microscopic 3-D picture of the membrane. (c) Example of tuning properties of a 1.56-μm MEMS-VCSEL with >20-nm tuning. TEC, thermoelectric cooler; NTC, negative temperature coefficient thermistor.

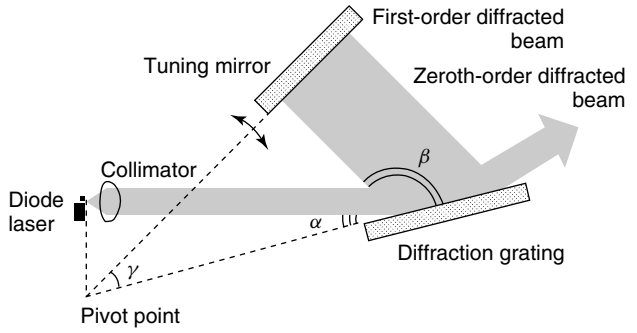

Figure 5 Optical diagram of an ECDL. Light at a wavelength λ emitted by the laser chip is collimated and is incident upon a diffraction grating with a period b. The first-order diffracted beam emerges at an angle to the grating, such that $\cos\alpha - \cos\beta = \lambda/b$, and is folded back into the cavity by an adjustable mirror. The round-trip distance traveled by light in the cavity must be an integer number of wavelengths. Continuous wavelength tuning results when both these conditions are met; this is accomplished by rotating the tuning mirror around a pivot point located outside the laser cavity, as shown.

an ECDL, one or both faces of the laser chip are anti-reflection-coated to eliminate optical feedback. The feedback is provided by a larger, external cavity. The cavity acts as a wavelength selector, picking a specific wavelength out of the usually broad gain spectrum of the semiconductor laser material. Several cavity configurations have been developed that differ in the method of tuning, component count, output beam characteristics, and output coupling efficiency. Figure 5 shows a frequently used external cavity type, known as the Littman configuration. It employs a diffraction grating as a wavelength discriminator. The first-order diffracted beam is folded back into the cavity by a mirror that acts as a tuning element – its angle and position determine the output wavelength. The grating also functions as an output coupler, producing the zero-order (reflected) beam whose angle and point of origin are independent of wavelength. Mode-hop-free single-frequency tuning ranges of over 1000 GHz have been demonstrated for an ECDL.[36] A spectrometer based on such a widely tunable laser is a very useful tool, in that it can acquire spectra of an entire molecular band in a single electronically controlled scan in a matter of seconds. Oh and Hovde,[37] for example, used a widely tunable 1.5-μm ECDL to record a spectrum of the $\nu_1 + \nu_3$ stretch-vibration combination band of acetylene.

To further enlarge the spectral range covered by a single laser, an optical frequency comb can be used. A frequency comb, generated from an ultrafast laser with femtosecond pulses, is made of tens to hundreds of thousand equally spaced spectral lines that constitute a frequency ruler over a spectrum that can be as large as one octave. The advent of frequency combs has revolutionized the time and frequency metrology,[38] making it possible to directly and easily link optical and microwave frequencies and thus to measure absolute optical frequencies (in terms of the SI second). Besides its application in frequency metrology, a stabilized frequency comb can also be a versatile spectroscopic tool, combining an excellent accuracy (the frequency of each comb line can be known with a high precision), a high spectral purity (each comb line has a narrow linewidth), and, at the same time, a broad spectral coverage, allowing a single laser source to perform spectroscopy over an octave spectrum.[39] The tremendous number of comb lines simultaneously available opens new perspectives for broadband spectroscopic analysis but requires new sophisticated schemes to extract the spectroscopic information corresponding to each individual comb line. The light transmitted through an analyzed gas sample can be spectrally resolved with either a grating spectrometer producing a one-dimensional dispersion pattern or a virtually-imaged phased array (VIPA) spectrometer that provides a higher resolution and a more compact two-dimensional dispersion pattern.[40] The development of massively parallel detection schemes has enabled the acquisition of broadband and high-resolution atomic and molecular spectra in submillisecond timescales using direct absorption and CRDS. In the direct absorption experiment of Diddams et al.,[40] two spectrally dispersive elements (a diffraction grating orthogonal to a VIPA disperser) were simultaneously used to disperse the spectrum, which was finally imaged onto a CCD camera. The resulting array of dots detected on the camera pixels represents the individual comb lines, which are separated by the comb repetition rate, in the order of 1 GHz. These lines can be accurately tuned by scanning the comb repetition rate or offset frequency, enabling to perform high-resolution molecular spectroscopy. In the cavity ring-down experiment of Thorpe et al.,[41] 125 000 optical comb components of a broadband frequency comb were simultaneously coupled into a high-finesse cavity to create the simultaneous ring-down decay of 125 000 individual cavity modes. This was used to simultaneously measure C_2H_2, O_2, H_2O, and NH_3 spectra across a 100-nm bandwidth in the visible and NIR spectral regions.

NIR diode lasers often come in compact sealed packages that include a convenient fiber-coupled output. Thus, the probe light can be delivered from a single source to several sampling locations. Likewise, the radiation passing through the sample can be returned to a detector via a fiber, sometimes even the *same* fiber (Figure 6).

A general problem that is faced in NIR trace-gas sensing is interference by water vapor. Long path lengths do not help here, as they increase not only the signal of interest but also the interfering absorption.

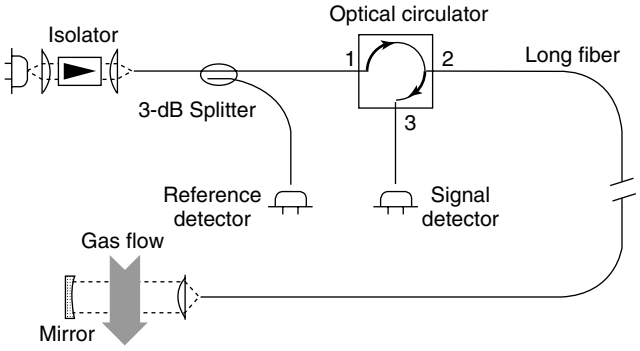

Figure 6 Schematic of an NIR diode laser spectrometer using a single fiber to deliver the light to and from the sampling location. The reference detector monitors the laser output power during frequency scans. The optical circulator transmits light from port 1 to 2 and from 2 to 3 and is used to route the returned beam to the signal detector.

Multicomponent spectral fitting algorithms have been developed that can resolve weak absorption lines of interest in the presence of heavy interference by a known gas. However, the problem becomes far more severe when the identity of the interfering species is unknown. An efficient way to reduce interference from H_2O (and from other potential interferents) is to reduce the sample pressure: all lines become narrower when the pressure is decreased, so that the overlap of nearby absorption lines is reduced accordingly.

3.3 Fundamental Band Detection with Mid-infrared Lasers

Lead-salt diode lasers have been developed for operation at wavelengths from 3 to 30 μm. They typically deliver 10–500 μW of output power in a near-diffraction-limited beam and can be tuned by temperature or current control. These lasers are based on PbS, PbSe, or PbTe semiconductors and generally require cooling near the temperature of liquid nitrogen, although a continuous wave (CW) operation has been achieved at temperatures as high as 195 K.[42]

MIR spectrometers employing lead-salt diode lasers have shown perhaps the most impressive performance to date in terms of minimum detectable gas concentration. There are four reasons for this. First is the very high absorption strength of the fundamental molecular vibrational bands. For example, carbon dioxide at a 3.3 ppm concentration in air (which is roughly 100 times lower than its typical ambient level) will cause absorption of 15% at 4.23 μm over a 1-m path. Such macroscopic absorption signals can be easily measured even without sophisticated signal processing techniques. Second, lead-salt diode laser spectrometers use cryogenically cooled InSb or HgCdTe detectors with noise-equivalent powers in the range of 0.5–50 pW $Hz^{-1/2}$, and although the lead-salt lasers produce less output power than their NIR counterparts, there is still enough light to render the detector noise virtually nonexistent and allow shot-noise-limited detection. Third, near-diffraction-limited beam characteristics of lead-salt diode lasers allow beam shaping and propagation over long distances; this makes it possible to use multipass cells or remote sampling in open air. Fourth, lead-salt diode lasers have FM capabilities similar to those of NIR diode lasers, allowing the use of harmonic detection and two-tone modulation techniques – efficient methods of noise bandwidth reduction, to be discussed in Section 4.3.

These advantages add up to a real-world instrument performance that is impressive.[5] Schiff et al.[43] report the detection limit 75 ppt for airborne measurements of HNO_3 in the continental boundary layer with a response time of 3 min. Werle et al.[44] achieved a detection limit of 10 ppt for NO_2 under laboratory conditions using a signal averaging time of 25 s.

Although well entrenched in a spectroscopic laboratory, lead-salt diode lasers are seldom used in industrial applications. Preventing their wide acceptance are several important practical drawbacks. Perhaps the most serious one is the large manufacturing spread of operating wavelengths. The situation is aggravated by the fact that each individual laser has a rather limited tuning range, typically 100 cm^{-1} with temperature control, and that the range itself is not free of mode hops. This makes it difficult to find a laser chip that actually tunes to a specific wavelength – a situation potentially catastrophic in applications where there is a limited choice of absorption lines free from interference by other lines, e.g. detection of formaldehyde.[45]

A more subtle problem with lead-salt diode lasers has to do with thermal cycling, a process in which a laser is simply warmed up to room temperature and then cooled back to its normal operating temperature. The simple process tends to cause irreversible changes in prior laser-tuning characteristics and emission wavelength.

Despite these and other technical difficulties, several specialized trace-gas sensors based on lead-salt diode lasers have been developed for field use. These instruments show excellent performance, proving just how effective the use of an MIR diode laser can be. For example, Webster and May[46] reported the design and operation of a fully automatic, compact sensor for the measurement of five trace gases in the lower stratosphere on board an airplane. Their instrument houses four lasers and four detectors mounted on the same liquid-nitrogen-cooled platform, beam shaping optics, a compact multipass absorption cell with 80-m path length, analog electronics, and a computer-controlled data storage system. It is capable of detecting optical

absorption as small as 10^{-5}, which corresponds to detection limits in the range of several tens of ppt for species such as HCl, NO_2, HNO_3, CH_4, and N_2O. Podolske and Loewenstein[47] report construction and performance of a similar instrument that uses an additional, 'zero', beam for removing the background absorption signal caused by gases within the instrument case. Both instruments employ wavelength modulation (WM) and second harmonic detection to achieve high sensitivity.

Quantum cascade laser (QCL) is a more recent technology for MIR light generation. In contrast to lead-salt diode lasers in which the emitted wavelength is defined by the material energy bandgap (interband transition), light generation in a QCL results from electronic transition between bound states created within the conduction band (intersubband transition) by quantum confinement in alternating ultrathin layers of semiconductor material (quantum wells). The emitted photon energy is determined by the thickness of the wells and barriers only and not by the material bandgap. Therefore, QCLs can be manufactured from technologically mature semiconductor compounds used in the widespread NIR telecom-grade lasers, e.g. standard indium phosphide (InP) technology, and the emission wavelength can be tailored by bandgap engineering. Since their first demonstration in 1994,[48] QCLs have shown a tremendous development, and InP-based QCLs have now been demonstrated across a broad wavelength range, from 4 μm up to the terahertz region at 300 μm. Other materials, e.g. InAs/AlSb,[49] are also investigated to reach the spectroscopically important 3- to 5-μm atmospheric window where many species of interest can be detected with limited interference from H_2O and CO_2.

QCLs generally require cryogenic cooling for CW operation, but room-temperature operation is achieved in pulsed mode, and even in CW in some spectral ranges.[50] QCLs were first fabricated as solitary Fabry–Perot (multimode) lasers, but single-mode operation was then achieved with the use of a DFB grating.[51] More recently, external-cavity quantum cascade lasers (EC-QCLs) have also been realized, with a tuning range of over 15% of the central wavelength.[52] Such a broad spectral coverage opens new perspectives for the detection of larger molecules with unresolved absorption spectra, such as freons, acetone,[53] ethylene glycol, and dimethyl methylphosphonate (DMMP).[54]

With their high output power (up to several hundreds of milliwatt) in single-mode operation, QCLs are particularly attractive for gas-sensing applications and have been used with the most sensitive spectroscopic techniques, including long path length,[55] balanced detection,[56] WMS,[57] FMS,[58] OAS,[59] and CRDS,[60] and their room-temperature operation capability (at least in pulsed mode) makes these lasers well suited for field applications.[61]

3.4 Diode Laser Frequency Conversion

An alternative technique for producing spectroscopic MIR light is laser difference-frequency generation (DFG). Two laser beams at different frequencies combined in a nonlinear material with suitable dispersion characteristics can generate a beam at the difference-frequency ('idler'). Narrow emission spectra of the two lasers, usually referred to as 'pump' and 'signal', translate into a similarly narrow spectrum of the idler wave. Idler wavelength tuning is accomplished by tuning of the pump laser or signal laser, or both (Figure 7).

In the early demonstration of this method by Pine,[63] an argon-ion laser output and a dye-laser output were combined in bulk lithium niobate to produce a narrow band (15 MHz), 2.2–4.2 μm tunable radiation. However, NIR diode lasers can now be used instead,[64] making it feasible to construct compact MIR spectrometers that operate at room temperature (Figure 8). Thus, the convenience and practicality of NIR diode laser technology are combined with the analytical power of MIR spectroscopy in a single instrument. Such an instrument inherits the single-frequency operation and high speed modulation capabilities of diode lasers and takes advantage of their relatively wide tuning range. For example, a typical 780-nm diode laser (Table 2) can be tuned over 20 nm, or 2.6% in wavelength, by temperature control, without an appreciable change in output power. When the output of such a laser is down-converted by mixing with a 980-nm diode laser, the tuning range in frequency units remains the same, in this case a very significant tuning range 3.6–4.1 μm, or 13% in wavelength.

The practicality of diode-pumped MIR frequency conversion received a significant boost from the development of novel nonlinear materials, such as periodically poled lithium niobate ($LiNbO_3$), called PPLN, lithium tantalate ($LiTaO_3$), and potassium titanyl phosphate ($KTiOPO_4$, or KTP) at wavelengths in the 2.5- to 5.2-μm spectral region.[66] Quasi-phase-matching properties of each of these crystals can be engineered for interaction of any pump and signal wavelengths within the transparency range of the crystal, allowing significant flexibility in the choice of laser sources.[67]

Although routinely used for spectroscopy and gas detection, DFG in bulk nonlinear crystals is characterized by low conversion efficiency, typically in the range of 0.002–0.05% $W^{-1}\,cm^{-1}$.[68] A detailed quantitative theory of this nonlinear optical process, developed by Boyd and Kleinman[69] or Chu and Broyer[70] is beyond the scope of this review chapter, so we simply state that

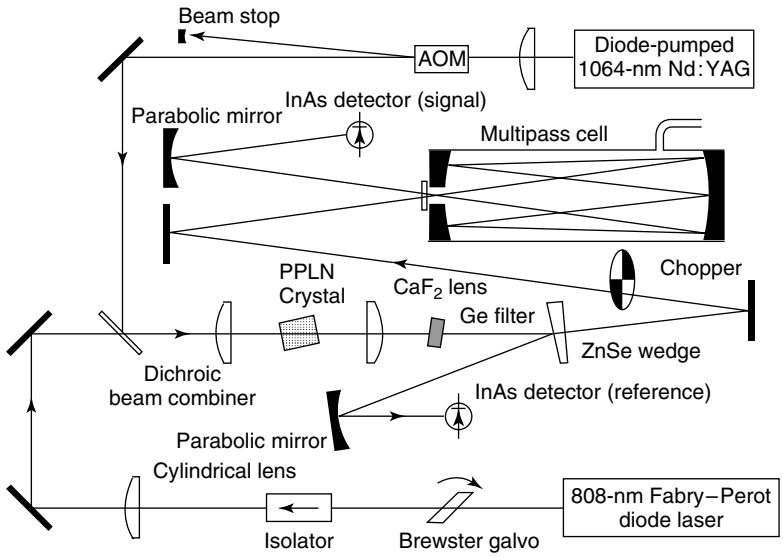

Figure 7 Schematic of difference-frequency spectrometer. A free-running Fabry–Perot diode laser at 808 nm, the 'pump', is mixed with a diode-pumped Nd:YAG laser, the 'signal', in a periodically poled $LiNbO_3$ (PPLN) crystal to produce a 3.4-μm tunable radiation. An antireflective-coated germanium filter blocks the residual pump and signal light.[62] (Reproduced from Ref. 62. © Springer, 1995.)

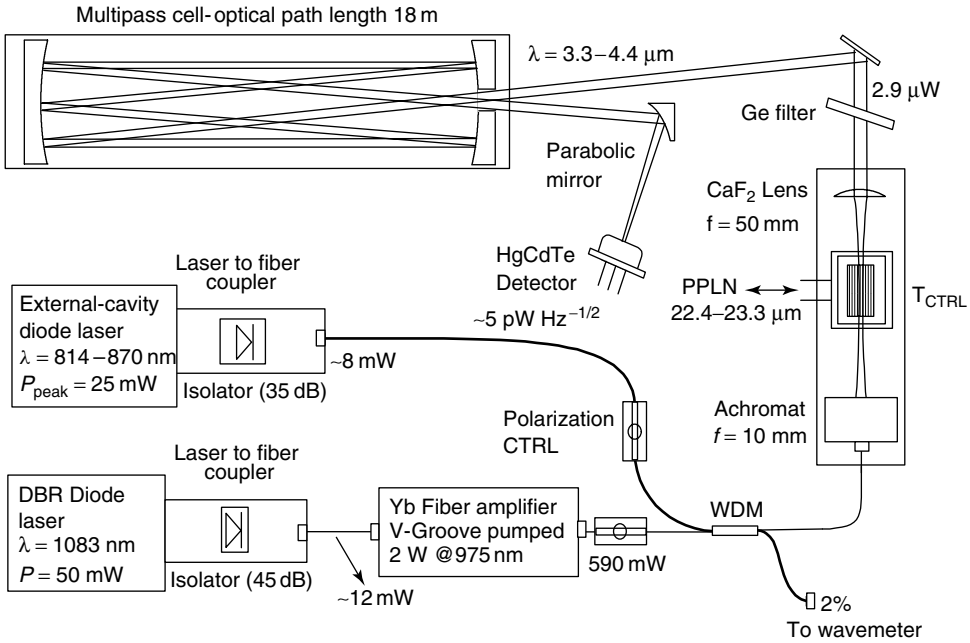

Figure 8 Portable diode-pumped difference-frequency spectrometer for detection of trace gases.[65] DBR, distributed Bragg reflector. (Reproduced from Ref. 65. © Springer, 1999.)

the maximum idler power generated in a given crystal is proportional to the product of crystal length, pump power, signal power, and the squared second-order nonlinear coefficient of the crystal. Maximum DFG output power is achieved by means of optimal focusing,[71] for which any further increase in beam intensity through tighter focusing is offset by a decrease in interaction length due to diffraction, resulting in no gain in output power. For DFG radiation longer than 5 μm, it is possible to use birefringent bulk nonlinear optical materials, such as $AgGaS_2$, $AgGaSe_2$, GaSe, and in the future, quasi-phase-matched GaAs.

The trade-off between beam size and interaction length can be eliminated altogether in guided-wave DFG. Tight

optical confinement of pump and signal radiation near the waveguide core creates a region of high intensity and good modal overlap, which are both maintained throughout, and independent of, the length of the waveguide.[72] Interaction length is now limited by the length of the waveguide, not diffraction. Guided-wave parametric processes, such as OPO (optical parametric oscillator), SHG (second harmonic generation), and DFG, have been demonstrated in PPLN, $LiTaO_3$, and KTP. In $LiNbO_3$, for example, a waveguide can be formed by titanium in-diffusion[73] or a $^{+}Li \longleftrightarrow {}^{+}H$ ion exchange.[74] The latter process is normally followed by several hours of annealing at an elevated temperature to create a graded index distribution.

A DFG waveguide designed to carry a single spatial mode at the idler wavelength is necessarily multimode at the shorter, pump and signal wavelengths. The presence of multiple spatial modes complicates the waveguide phase-matching characteristics considerably. For example, a TM_{00} (transverse magnetic, fundamental) mode at the signal wavelength will interact with TM_{02} and TM_{10} modes at the pump wavelength, but not with TM_{01} or TM_{11} modes. Efficient and reproducible fundamental-mode excitation of a DFG waveguide was first achieved by Chou et al.,[75] who used the combination of a mode filter and an adiabatic taper (Figure 9). An improved device featuring separate inputs for the pump and signal beams followed by a directional coupler has also been demonstrated.[76] DFG waveguides have been used to build viable sources of MIR radiation for spectroscopic purposes.[77] Other details about MIR DFG sources can be found in the review papers of Wächter and Sigrist[78] and Fischer and Sigrist.[79]

In the last years, DFG processes have gained an additional interest for the generation of MIR optical frequency combs. Following the advent of NIR frequency combs (Section 3.2), it has rapidly appeared

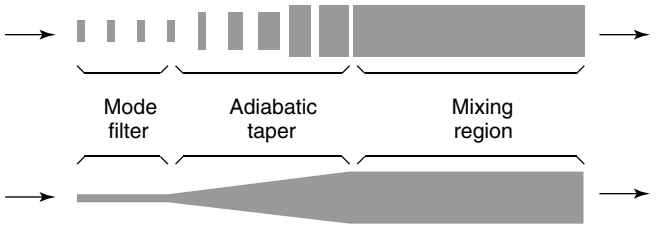

Figure 9 Alternative geometries of a tapered waveguide for difference-frequency mixing. Shaded regions indicate material with higher index of refraction. Laser light is launched into the mode filter that carries a single (fundamental) spatial mode. The mode size is then adiabatically converted to fit the mixing waveguide, which is multimode. Periodic segmentation[75,76] of the waveguide acts to reduce the effective index. It also provides independent control of the effective waveguide width and depth. (Reproduced with permission from Refs 75, 76. © The Optical Society of America, 1996 and 1998.)

that direct comb synthesis in the MIR region would be a breakthrough in frequency metrology as well as for absolute frequency molecular spectroscopy. So far, no laser is able to directly generate a MIR comb, hence indirect means have to be implemented. Maddaloni et al.[80] have demonstrated a MIR optical frequency synthesizer generated from DFG between a NIR frequency comb and a tunable CW laser in a PPLN crystal. The resulting MIR comb can extend from 2.9 to 3.5 μm (in 180-nm wide spans) with a 100-MHz mode spacing and has an overall power of about 5 μW. By phase-locking the pump laser to the NIR comb and referencing the NIR comb to a microwave frequency standard, the frequency of each MIR comb line is known and the MIR comb can act as a frequency ruler for high-precision spectroscopy. In a different approach, Foreman et al.[81] produced a 3.39-μm frequency comb by DFG between two spectral regions of a visible–NIR Ti:sapphire comb. By mixing approximately 12.3-mW average power contained within a 7-nm bandwidth at 670 nm with a 10-nm-wide spectral region centered at 831 nm (7.8-mW average power) into a temperature-controlled PPLN crystal, the generated offset-free MIR comb has a bandwidth of 270 nm centered near 3.4 μm. Approximately 10 μW of average power was measured through a 50-nm bandwidth interference filter, corresponding to nearly 600 pW per comb mode. We should notice that in this realization involving two pulsed spectral components, a temporal superposition of the two pulses into the PPLN crystal has to be ensured for the DFG process to take place. This was achieved using a prism-based delay line.

4 TECHNIQUES FOR THE MEASUREMENT OF SMALL GAS CONCENTRATIONS

4.1 Long Path Length and Cavity-enhanced Spectroscopy

Gas sensors often deal with gas concentration and sample size that are so small that the detected full-scale absorption signal is indistinguishable from system noise. This is no surprise since most photons in the probe beam pass through the sample without being absorbed. If one were able to somehow 'recycle' these unabsorbed photons, by forcing them to pass through the sample many times, one would obtain better contrast between signals on and off resonance of the molecular transition. Two different forms of this idea have been developed to date.

Long path length spectroscopy, not to be confused with remote sensing or fence-line monitoring,[82] refers to the use of an optical set-up that provides multiple passes of the probe beam through a relatively small sample volume.

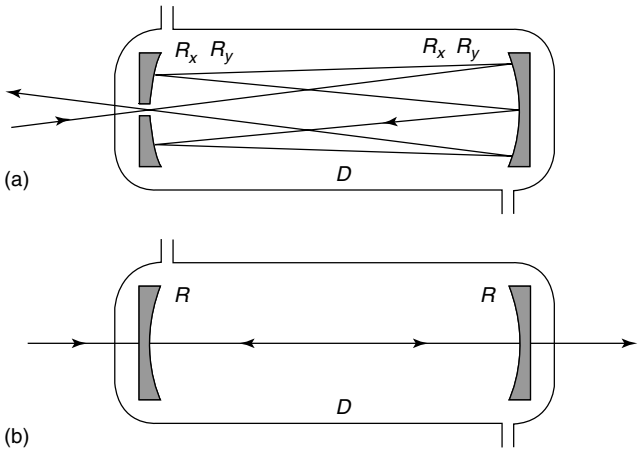

Figure 10 (a) Schematic of a multipass cell. The standard Herriott cell has two spherical mirrors separated by nearly their radius of curvature $D \approx R_x = R_y$. Unlike with the confocal cavity (b), a resonance does not occur in the multipass cell because the beam never hits the same spot twice on any mirror before it exits through the coupling hole.

An example is the Herriott cell, a device with two identical spherical mirrors facing each other and separated by nearly their radius of curvature (Figure 10). A probe beam launched through a hole in one of the mirrors at an angle to the optical axis completes a certain number of passes between the mirrors and exits through the same hole. The mirror curvature, applied to the beam at each reflection, keeps it from diverging, as if in a cavity. The beam bounce pattern and path length can be controlled by adjusting the mirror separation. The picture is deceptively simple, but certain design rules must be followed to ensure that the beam exits the cell after a controlled number of passes, especially in the case of astigmatic mirrors.[83] The number of passes can routinely exceed 100, thus providing a commensurate improvement in signal strength (Figure 11). It is important to recognize that mirrors are not perfect, and a small portion of the probe light is lost to absorption and scattering each time the beam bounces. Optical throughput of the cell thus decreases exponentially with the number of passes, whereas the detected peak-to-peak absorption only increases linearly (in the small-signal limit) with the number of passes.

Several configurations of the multipass cell are available, which offer different mirror counts, input and output ports, and beam patterns. They can be sealed, for the measurement in static gas samples or controlled gas flows, or open to ambient air. Performance of long path length multipass cells, especially those with dense beam patterns, suffers from optical interference ('fringes') because of light scattering by the cell mirrors. The fringe magnitude is sensitive to optical alignment and is typically on the order of 0.01–0.1% full-scale transmission (Figure 11). Mirror drift and vibration can also become a problem, as they modulate the cell transmission. Mirror vibration, on the other hand, reduces the effective magnitude of interference fringes, as it scrambles the phase of optical feedback within the cell.[4]

Cavity-enhanced spectroscopy is another method to increase the magnitude of absorption signal when only a small concentration of gas sample is available. Although its implementation and treatment are different from those

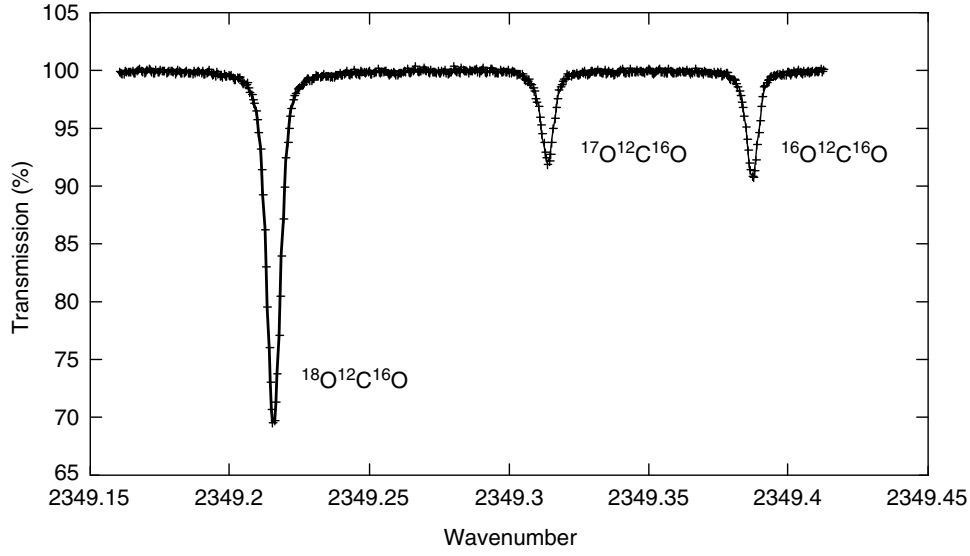

Figure 11 Direct-absorption spectrum of three different isotopes of natural CO_2 in air at a pressure of 3.6 kPa in an 18-m multipass cell. The probe beam makes 90 passes between the cell mirrors that are 20 cm apart. Given the cell transmission of 33%, the overall gain in signal strength is 30.[85] Interference fringes, due to light scattered by the mirrors, can be seen in the baseline. (Reproduced from Ref. 85. © Springer, 1998.)

described above for the multipass cell, the similarity is evident if one considers the idea of 'recycling' photons in the probe beam. In this method, a weakly absorbing gas sample is placed inside a cavity, and the cavity is tuned to resonance with the probe beam, e.g. by a piezo-driven cavity mirror. At the peak of resonance, the cavity photon lifetime significantly exceeds the cavity round-trip time, thus increasing the probability of interaction with gas molecules in the sample. The effective number of passes between cavity mirrors, N, constitutes the improvement in the magnitude of absorption signal and is proportional to cavity finesse, F, which can be made rather high (Equation 12)[86]:

$$N = 2\frac{F}{\pi} \tag{12}$$

This approximation is good for weak absorption signals. A point to consider here is that increased gas absorption acts to reduce ('spoil') the cavity finesse. This leads to nonlinear distortion of the observed molecular lineshapes, making a quantitative measurement difficult. Another point to consider is that the cavity must be kept in resonance with the probe beam when the wavelength is tuned. A feedback loop is often used, which adjusts cavity length to track the changes in probe wavelength.[62] The rate of this electromechanical adjustment is much too slow to keep up with the laser tuning rate normally used for sensitive spectroscopy (more on this in Section 4.3).

Another form of cavity-enhanced spectroscopy is CRDS.[87–92] This technique is based on the measurement of the decay rate of the light intensity inside the cavity. Once the optical power injected into the cavity from a laser source is sufficient, the input light beam is interrupted and the decay of the light power escaping the cavity through one of its mirrors is monitored using a photodiode. The transmitted light intensity decays exponentially in time, with a time constant (the ring-down time) that is directly related to the optical losses in the cavity. Owing to the additional intracavity losses induced by an absorbing gas, the cavity ring-down time τ is reduced compared to its value τ_0 for the empty cavity, and the sample absorption is directly obtained from the difference between the decay rates of the empty and filled cavities (Equation 13):

$$\alpha(\lambda) = \frac{1}{c}\left[\frac{1}{\tau(\lambda)} - \frac{1}{\tau_0}\right] \tag{13}$$

One of the advantages of CRDS compared to traditional absorption methods is that it measures the time constant of the exponential decay of the cavity, and this parameter is independent of intensity variations of the input source. Therefore, unlike traditional absorption spectroscopy, CRDS is not affected by laser intensity noise. Furthermore, with typical mirrors with 99.995% reflectivity, an effective path length of several kilometers can be achieved, leading to a minimum detectable absorption loss in the $10^{-12}\,\mathrm{cm}^{-1}\,\mathrm{Hz}^{-1/2}$ range.[93]

An interesting, and remarkably simple, method to increase effective path length through a gas sample has recently been demonstrated by Tranchart et al.[94] It involves the use of a broadband integrating sphere whose inside walls diffuse light rather than reflecting it. Effective path length for the probe beam inside the sphere is then given by Equation (14):

$$L_{\mathrm{eff}} = \frac{4R}{3(1-\rho)} \tag{14}$$

Here R is the sphere radius and ρ is the diffuse reflection coefficient. Highly reflective walls ($\rho \to 1$) make it possible to obtain several meters of effective path length from a sphere as small as 10 cm in diameter. This method does not require sophisticated alignment of the probe beam into the sphere but has the disadvantage of low detected power that is proportional to the ratio of the detector active area to the inside surface area of the sphere. Additionally, the effective path length depends on the sphere diffusivity, which might be subject to degradation over time due to dust or aging of the sphere's internal surface. The limiting factor in such a diffusive geometry arises most often from random laser speckles and self-mixing interference, as discussed by Masiyano et al.[95]

4.2 Balanced and Balanced Ratiometric Detection

Laser intensity noise and drift may limit the sensitivity with which absorption signals are measured. This is particularly true for gas lasers, or externally pumped solid-state ring lasers, where output power fluctuations induced by acoustic vibration and variations in pump power can exceed 1% full scale. Balanced detection may be used to recover small absorption signals in this situation. Noise detected in an equal-intensity replica of the probe beam, such as that created by a variable-ratio beam splitter, is subtracted from noise detected in the probe beam, thus leaving only the uncompensated weak absorption signals of interest. A variable-ratio beam splitter can be made by placing a polarization rotator (a half-wave plate) in series with a polarizing beam splitter cube, as shown in Figure 12.

With the input polarization rotated about 45°, the beams emerging from the beam splitter cube carry equal amounts of power P and power noise ΔP. In the absence of absorption, the photocurrents generated by the (identical) signal and reference detectors can be subtracted to cancel each other exactly. If one of the

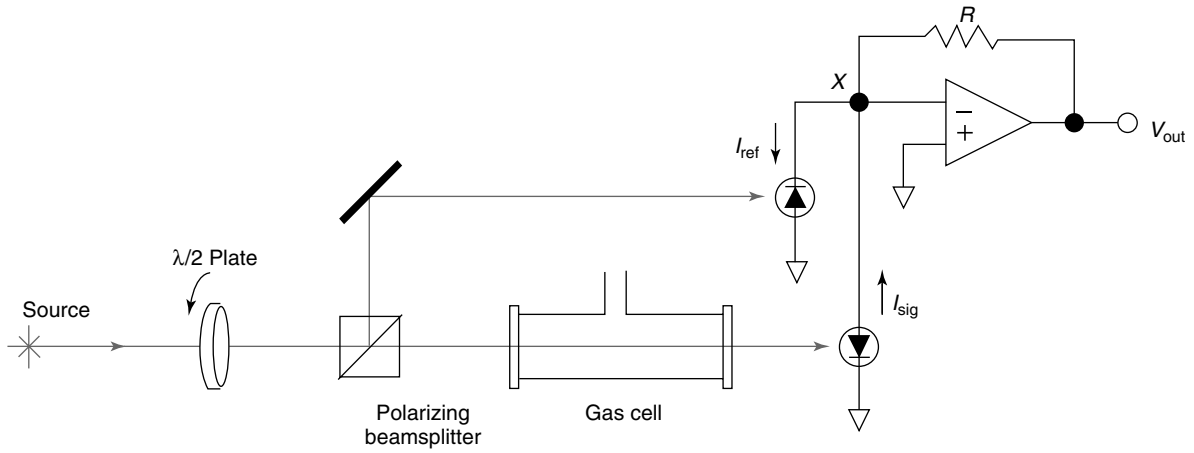

Figure 12 In the simple balanced detection method, a variable-ratio beam splitter (a combination of a half wave plate and a polarizing beam splitter) is used to send nearly equal amounts of optical power to the signal and reference detectors, bringing V_{out} to zero. The balance at the current-summing junction X is maintained despite the laser amplitude noise since the generated noise photocurrents are of opposite sign and nearly equal magnitude. An imbalance of photocurrents due to absorption in the signal beam results in a nonzero output.

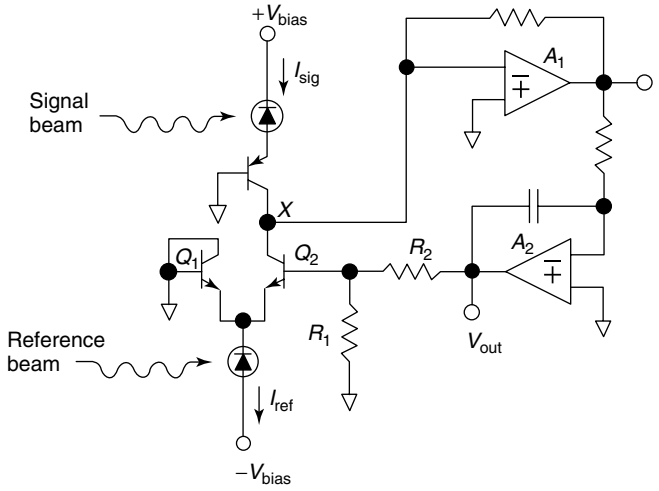

Figure 13 Circuit diagram of a balanced ratiometric detector. When currents at the summing junction X are balanced, the output of the error amplifier A_1 is zero, and the output of the integrator A_2 is proportional to $\ln(I_{ref}/I_{sig} - 1)$. A nearly perfect cancellation of noise photocurrents is achieved when $I_{ref} \approx 2I_{sig}$.

beams is attenuated due to small absorption a, by a gas, for example, the balance of photocurrents is disturbed, and a signal is seen at the output of the amplifier (Equation 15):

$$V_{out} = R(I_{ref} - I_{sig}) = aRSP + aRS\Delta P \qquad (15)$$

Here, R is the feedback resistance and S is the detector element response (responsivity) in amperes per watt. The second term constitutes noise, and the corresponding signal-to-noise ratio is $P/\Delta P$, independent of absorption a and limited basically by the quality of the probe beam. With the use of a single detector (no balancing), the signal-to-noise ratio would be a mere $aP/\Delta P$, i.e. absorption on the order of $a_{min} = \Delta P/P$ would be indistinguishable from noise. In practice, adjustment of the beam splitting ratio ('zeroing') is necessary to compensate for unequal response of the signal and reference detectors and difference in optical transmission of the signal and reference arms. Moreover, detectors must be sufficiently quiet to resolve fluctuations in probe power and must have equal delay times.

An advanced implementation of this method, proposed by Hobbs[96] and known as BRD, uses circuitry to compute a log ratio of photocurrents, rather than their difference, and to cancel noise currents at the same time. The analog divider, whose simplified schematic is shown in Figure 13, uses logarithmic conformance and tight symmetry of base-emitter curves of a matched transistor pair. The summing junction X is held at ground by an error amplifier A_1 whose output is integrated and applied to the base of transistor Q_2. When currents at the summing junction are balanced, the output of A_1 is zero and the output of A_2 is given by Equation (16):

$$V_{out} = \frac{R_1}{R_1 + R_2} \frac{k_B T}{e} \ln\left(\frac{I_{ref}}{I_{sig}} - 1\right) \qquad (16)$$

Here, k_B is the Boltzmann constant; T, the absolute temperature of the matched transistor pair Q_1Q_2; and e, the electron charge. This scheme provides nearly perfect cancellation of noise currents when the reference beam carries roughly twice the power of the signal beam. The signal-to-noise ratio is thus increased well beyond the $P/\Delta P$ limit of the simple balancing scheme described above.

Since the signal versus reference current balancing is performed by means of electronic feedback, no physical adjustment of the beam splitting ratio is necessary. However, the BRD differential response to absorption signals is nonlinear, in that it depends on the ratio of the signal and reference currents, which changes when the signal beam is partially absorbed. It also depends on temperature like the transistor base-emitter voltage, and additional compensation circuitry is needed to produce a useful output voltage V_{out}. Nevertheless, detection sensitivities presently achieved with BRD are quite stunning. Noise-equivalent absorbances as low as $2 \times 10^{-7}\,\mathrm{Hz}^{-1/2}$ have been demonstrated by Allen et al.,[16] close to the limit imposed by the laser shot noise.

4.3 Frequency and Wavelength Modulation Spectroscopy

The ability of a diode laser to change its emission wavelength with injection current, and to do so very rapidly, is one of the reasons why the diode laser has been so effective in spectroscopic applications. The wavelength change is driven by two effects. Current-induced heating of the semiconductor junction leads to change in optical length of the laser cavity and redshifts in the laser's broad gain curve; this constitutes 'coarse' tuning. The current also controls the carrier density, which in turn affects the cavity refractive index; this 'fine' tuning mechanism is normally at least 10 times less pronounced at low frequencies but becomes dominant at high frequencies (>1 MHz), where the thermal contribution is strongly damped and phase-shifted. The tuning response thus depends on the modulation rate and ranges from 2–3 GHz mA^{-1} at low frequencies to less than 300 MHz mA^{-1} at high frequencies in DFB lasers. In NIR VCSELs, the tuning response is one to two orders of magnitude larger. FM is always accompanied by amplitude modulation (AM), as the injection current also controls the laser output power (Equation 17):

$$E(t) = A\{1 + m\cos(\Omega t)\}\sin\{\omega t + \beta\cos(\Delta t + \Phi)\} \quad (17)$$

Here, $E(t)$ is the laser electric field; $\omega = 2\pi c/\lambda$, the laser frequency; and Ω, the modulation frequency. By analogy with radio communication, ω is the 'carrier' frequency. The quantities m and β are the amplitude modulation and FM indices, respectively, and Φ is the generally nonzero phase shift describing the phase lag between the applied current modulation and the resulting FM. Sine wave modulation of the diode laser has the effect of creating multiple sidebands in its otherwise nearly monochromatic emission spectrum. Each sideband is separated from the carrier by an integer multiple of the modulation frequency Ω, and its relative intensity depends on β.[97]

In FM *spectroscopy*, for example, Ω significantly exceeds the width of the gas absorption line under investigation, which is typically a few tens to a few hundreds of megahertz for the Doppler width of MIR transitions, and m and β are both small, so that only the two first-order sidebands, $\omega + \Omega$ and $\omega - \Omega$, have appreciable magnitude. After uniform attenuation, such as that encountered in nonresonant optical systems or media (e.g. imaging optics or vacuum), the sidebands add up coherently to the carrier and balance each other to produce a beam of nearly constant intensity, A^2. However, if the attenuation strongly depends on frequency, as is the case with most gases, one of the sidebands may become unbalanced and lead to the appearance of multiple harmonics of Ω in the detected laser intensity. The strength of absorption determines the magnitude of these harmonics, which may be measured separately and with high noise immunity by using a proper frequency demodulation. This is usually done while the laser carrier frequency ω is scanned in the vicinity of the absorption line of interest.

This detection technique was first applied by Bjorklund to a CW dye laser.[98] It proved extremely powerful and is widely used in diode laser spectroscopy today, sometimes in modified form such as TTFMS[99] and amplitude modulated phase modulation (AMPM) spectroscopy.[100] Owing to the requirement of a modulation frequency larger than the absorption linewidth, the FMS methods are most often used at reduced pressure, with linewidth in the range of tens to hundreds of megahertz.

The combination of FM with cavity-enhancement spectroscopy has led to outstanding detection sensitivities in trace-gas sensing. The technique is referred to as noise-immune cavity-enhanced optical heterodyne molecular spectroscopy (NICE-OHMS) and basically consists of coupling a frequency-modulated laser into a high-finesse cavity.[101–103] When the laser FM perfectly matches the cavity free-spectral range, each modulation sideband becomes resonant with a cavity mode, making the detection process insensitive to the laser frequency noise relative to the cavity. In this scheme, the cavity enhances the molecular response to the light field, and the FM technique is applied for shot-noise-limited signal recovery. Ye et al.[101] have shown a record noise-equivalent detection sensitivity of 5.2×10^{-13} at 1-s averaging obtained by the NICE-OHMS technique on the C_2HD (ν_2+3ν_3) $P(5)$ transition at 1064 nm using a solid-state diode-laser-pumped nonplanar ring Nd:YAG laser with a cavity finesse of 100 000. The NICE-OHMS technique has later been implemented with NIR ECDL[102] and DFB-QCL,[103] but the achieved sensitivity has not been as outstanding as in the original work of Ye et al.

Wavelength modulation spectroscopy (WMS) is really another form of FM spectroscopy, in which case the modulation frequency Ω is smaller than the gas absorption linewidth and the modulation index β is large.[104] The aforementioned sidebands are then present to a very high order and, by virtue of their small separation from each other, merge into a continuous spectrum. The detection is again performed at the first, second, or higher harmonics of Ω (using a lock-in amplifier for example) as the laser carrier frequency ω is scanned in the vicinity of a gas absorption line. WMS dominates applications that rely on relatively low-speed detectors and/or gas-sensing applications at atmospheric pressure conditions where absorption lines are typically a few gigahertz wide. The sensitivity of WMS is ultimately limited by the laser amplitude $1/f$ noise, but most often by interferometric noise (etalon fringes and/or laser self-mixing), even in presence of fringes reduction techniques as described in Section 1.

WMS is quite simple to implement and at the same time a sensitive technique for trace-gas sensing. The technique is easily applicable to any type of NIR semiconductor laser (DFB,[21,22] VCSEL,[27,28,31] or ECDL[37]) as well as MIR lasers (lead-salt diode,[5,46,47] QCL,[57] DFG[62]) through a direct modulation of the laser injection current. WMS can also be combined with long path length techniques to further improve the detection sensitivity.[5] In WMS, the gas concentration is most often extracted from the second harmonic ($2f$) signal of the laser modulation frequency f, but detection at higher harmonics may offer some advantages in some particular conditions, e.g. to better resolve overlapping lines.[105] The WMS$-2f$ signal depends not only on the sample absorption but also on the laser modulation parameters (the relevant parameter is the normalized modulation index $m = \Delta\nu_{\text{laser}}/\Delta\nu_{\text{line}}$, where $\Delta\nu_{\text{laser}}$ is the excursion of the laser instantaneous frequency and $\Delta\nu_{\text{line}}$ is the width of the probed absorption line). Therefore, the WMS method requires calibration. Two types of approaches are considered to analyze the gas absorption $2f$ signal to extract the gas concentration. In the first approach, the entire $2f$ lineshape is recorded, while the laser is slowly tuned across the absorption line, and the measured spectrum is fitted by a theoretical $2f$ lineshape.[27,31] In the second approach, only the on-peak $2f$ signal is measured, which is directly proportional to the absorption and thus to the gas concentration (in the limit of small absorbance). This approach is much less demanding in terms of data processing and is particularly well suited in simple, compact, low-cost gas sensors, where all the control and processing tasks can be realized using a simple microcontroller. However, it requires that the laser is continuously stabilized to the center of the analyzed absorption line in order to correctly measure the on-peak $2f$ signal. Conventionally, this line locking is performed using a second beam path through a reference cell containing the analyzed species, and the first harmonic ($1f$)[47] or third harmonic ($3f$)[106] signal is used as an error signal to provide feedback to the laser to maintain the correct wavelength. Alternatively, a different reference molecular species can be used, which has an absorption line close to the transition of the analyzed gas. The benefit is that the reference cell can be inserted directly in the laser beam, thus avoiding the need for a reference path and leading to a more compact set-up. Such an example is given by Chen et al.,[31] where some CH_4 lines were used as a wavelength reference for CO detection using a 2.3-μm VCSEL. For higher compactness, the reference gas was directly included in the cap of the photodetector.

4.4 Optoacoustic Detection

The optical power absorbed by a gas from the probe beam leads to local heating of the gas and inevitably generates a local pressure differential. The pressure differential can, in principle, be detected as an acoustic pulse, some distance away from the source in any direction. A train of acoustic pulses at a known frequency, such as that produced in a gas by a chopped beam, for example, constitutes an acoustic wave (a 'tone'), which can be detected using a microphone and a lock-in amplifier (Figure 14). Since the optical power absorbed from the probe beam depends on wavelength, a change in the intensity of the acoustic wave will result as the laser wavelength is tuned. Spectroscopy based on this principle is called opto-acoustic spectroscopy (OAS), or *photoacoustic spectroscopy* (PAS). In PAS, the optical power absorbed in the gaseous sample is measured via the local heating and subsequent acoustic wave rather than being inferred from the optical power transmitted through the sample, as measured in other conventional spectroscopic techniques. For this reason, PAS is a type of calorimetric technique and thus has an important advantage: in the absence of any absorbing gas, there is no acoustic signal at all and the technique is said to be background free.

PAS is generally used in one of the two following implementations[107]: in *pulsed-mode PAS*, each individual short acoustic pulse produced by a pulsed laser is detected and analyzed in the time domain and in *modulated PAS*, the amplitude (and phase) of the acoustic wave generated by a modulated laser (sine or square wave modulation) is measured using a lock-in amplifier. Nowadays, modulated PAS is the most commonly used method. As the generated photoacoustic (PA) signal is proportional to the energy absorbed in the gas sample during a modulation cycle, the signal is inversely proportional to the modulation frequency f ($1/f$ dependence). External acoustic noise is an important issue in PAS, as

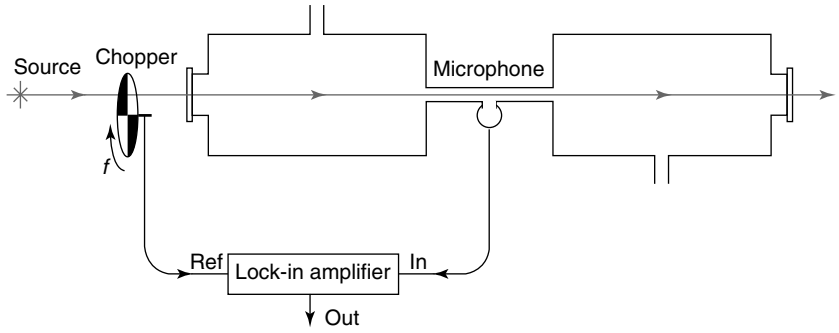

Figure 14 Simplified schematic of an optoacoustic trace-gas detection system using a resonant acoustic cell. The beam is chopped at a frequency f, and a synchronous acoustic signal is detected by a microphone and a lock-in amplifier. Laser WM on and off of the gas absorption line can produce an acoustic signal in much the same way as a chopped beam that is tuned to the line center.

it may add a parasitic contribution to the real gas absorption signal, even if its random phase relative to the laser modulation makes it effectively filtered away by the lock-in amplifier. In order to reduce the influence of acoustic noise, operating a PA sensor at higher frequency (some kilohertz) is preferred, as ambient noise is predominantly composed of low-frequency noise. In order to compensate the associated $1/f$ signal reduction, PA cells are most often designed as an acoustic resonator,[107–112] in which a standing wave is created when the laser is modulated at a resonance frequency of the cavity, and the PA signal is enhanced by the resonance quality factor Q in comparison with a nonresonant configuration. In that case, the method is referred to as modulated resonant PAS. Different modes (radial, azimuthal, longitudinal) of a cylindrical acoustic resonator can be used, as well as Helmholtz resonators.[110] The theory of the generation and detection of the PA signal in a cylindrical cell has been extensively discussed (see, for example, the books by Sigrist,[107] Bernegger,[110] Kreuzer,[113] and Dewey[114]) but is beyond the scope of this chapter. Basically, one can mention that the PA signal scales with the incident laser power, but also depends on a proportionality coefficient (called the cell constant) that describes the conversion from optical to acoustic energy in the PA cell and depends on the sensor geometry (in particular, the cell dimensions, the overlap integral between the laser beam and the excited acoustic mode, the position of the microphone, and some physico-chemical parameters of the gas mixture). Therefore, one of the key points in the development of a PA sensor is to properly design the PA cell, i.e. to maximize the cell constant while minimizing the impact of interfering synchronous acoustic signals (such as those generated by the slightly absorbing windows and walls of the sample cell), as well as the influence of acoustic noise. For this purpose, PA cells are often designed with input/output acoustic rejection filters.

As an alternative to pulsed-mode and modulated PAS, a third variant of photoacoustics, which consists of matching the pulse repetition rate with the resonance frequency of the PA cell, has been recently proposed by Bartlome et al.[115]

Since the optoacoustic signal is proportional to the beam intensity, the method has been used primarily with high-power infrared lasers, such as CO_2[108] and CO[110] lasers, and commercial instruments have been developed based on CO_2 laser.[116] While lower-power diode lasers such as NIR DFB lasers and MIR QCLs are now being used,[53,59,106,109,111,112,117] VCSELs are poorly suitable for PAS because of their much lower optical power. Surprisingly, the WM capabilities of diode lasers have found an elegant use in OAS – periodic tuning of the laser beam on and off the line resonance is also a good way to generate an acoustic wave. The theory for WM optoacoustic signal generation involves coupled heat transfer and the Navier–Stokes equations[118] and is beyond the scope of this review. However, the harmonic signals obtained in WM-OAS are very similar to those obtained in standard WM spectroscopy with optical detection.[119]

Another outstanding feature of PA techniques is their achromaticity: the response of a PA sensor is usually independent from the laser excitation wavelength (apart from very specific cases involving particular gas mixtures as explained in the next paragraph). It means that the same PA detector can be used with any type of lasers and at any wavelength, from ultraviolet to MIR, with identical performances in terms of cell response per unit absorption and incident optical power (provided that a suitable window material is used in the PA cell). This is definitively not the case for other high-sensitivity laser spectroscopy techniques, such as WMS/FMS and CRDS, which make use of optical detection that has poorer performances in the MIR region. Indeed, not only the sensitivity of MIR photodiodes is strongly reduced in comparison to NIR but also MIR detectors require low-temperature operation and are much more expensive than NIR detectors.

Despite its numerous advantages, PAS is an indirect technique, i.e. the laser optical energy absorbed by the molecules is not directly measured, but is determined through an indirect effect, which is the acoustic wave generated in the sample due to its thermal expansion. The conversion from optical to thermal energy, therefore, depends on some physico-thermal properties of the sample (not only from the analyzed species but also and mainly from the buffer gas). Consequently, PAS is not an absolute method and a calibration is essential. The dynamics of the relaxation of the excited molecules (in particular, vibration-to-translation relaxation processes) plays a major role in the generation of the PA signal. While this relaxation can be assumed instantaneous in most cases, since it is much faster than one period of the laser modulation, it turns out that it becomes much slower in some particular gas mixtures, and the corresponding long relaxation time can strongly influence the generation of the PA signal. As a few examples, Schilt et al.[111] showed that the response of a CH_4 PA sensor based on a 1.65-μm DFB laser and a PA cell resonating at ~1 kHz was reduced by more than one order of magnitude when the measurement was performed in a dry O_2 buffer gas compared to the case of pure N_2, and the signal was already strongly reduced in dry N_2/O_2 mixtures containing only a few percent of O_2. An unusual parabolic response of the sensor with respect to the methane concentration was also observed as a result of these relaxation effects. A similarly severe reduction of the PA response was reported by Veres et al.[112] for the detection of CO_2 in dry N_2 using a 1.43-μm ECDL and a 4-kHz resonant PA cell. In all cases, the presence of water vapor, even at low concentration, acts as a catalyst to hasten the molecular relaxation, which strongly enhances the PA response to the analyzed concentration.[117]

Quartz-enhanced photoacoustic spectroscopy (QEPAS) introduced by Kosterev et al.[106] is a variant of PAS, which maintains its main characteristics with the benefit of a quartz tuning fork (QTF) acting simultaneously as an acoustic sensor (instead of the traditional microphone) and as a miniature acoustic resonator (thus replacing the bulky PA cavity used in conventional PAS). This leads to an ultracompact, robust, and cost-effective trace-gas sensing module. QEPAS sensors are based on a high quality factor quartz resonator mass-produced as a frequency reference for clocks and watches. The resonance frequency of commercially available QTFs is 32.8 kHz compared to the operation frequency of a few kilohertz in conventional PAS. This makes QEPAS sensors insensitive to ambient acoustic noise, which often limits PAS sensitivity. The reduction of the PA signal associated with the high QTF resonance frequency (because of the $1/f$ dependence) is compensated by the high Q-factor of the QTF (from a $Q = 10^5$ in vacuum to $Q = \sim 10^4$ at atmospheric pressure) compared to PAS resonators with a Q-factor ranging from a few tens to several hundreds.[111,112,116] Hence, QEPAS can achieve a comparable sensitivity as conventional PAS, but with important benefits such as smaller size and reduced ambient acoustic noise impact. So far, QEPAS has been demonstrated with several simple molecules[106,117] using a single ro-vibrational line in fundamental MIR absorption bands (e.g. CO, N_2O, H_2CO, C_2H_6) or in NIR combination bands (e.g. NH_3, CO_2, HCN, H_2S, C_2H_2), as well as with larger molecules with broad, unresolved absorption spectra, such as acetone and freons.[53] The main difference in the implementation of QEPAS with narrow-line molecules and broadband absorbers is that WM at half the QTF resonance frequency with second harmonic ($2f$) detection and reduced pressure operation is applicable for target analytes with well-resolved absorption lines, whereas amplitude modulation at the QTF frequency and detection at the same frequency is necessary for molecular species with unresolved, congested spectra.

5 EXAMPLES OF TRACE-GAS SENSORS

Here, we describe practical embodiments of three types of laser spectroscopic sensors described in Section 3. These are sensors based on NIR semiconductor lasers, lead-salt diode lasers, and diode laser frequency conversion. We have selected one instrument in each category as an example. These instruments have either stimulated a development of a broad range of similar sensors and related measurement techniques or are an example of how multiple elements of the developed sensor technology function together in a complete spectroscopic instrument.

5.1 Gas Sensors Based on Near-infrared Diode Laser Overtone Spectroscopy

Intense development of gas sensors based on visible and NIR semiconductor lasers has been reported by groups in the USA, Europe, and Japan.[83,96] Applications in which these sensors find increasing use are combustion diagnostics, landfill emissions monitoring, natural-gas leak detection, optical sensing of flows, and industrial process control. One of the first applications of an NIR diode laser to gas detection was reported in 1992 by Uehara and Tai.[21] Figure 15 shows a schematic diagram of a spectrometer built for the purpose of detecting methane in ambient air; it uses the same transmitter design in two remote detection schemes. The transmitter employs a 1.665-μm InGaAsP DFB diode laser developed specifically for the detection of methane in the $2\nu_3$ stretch vibration overtone band.

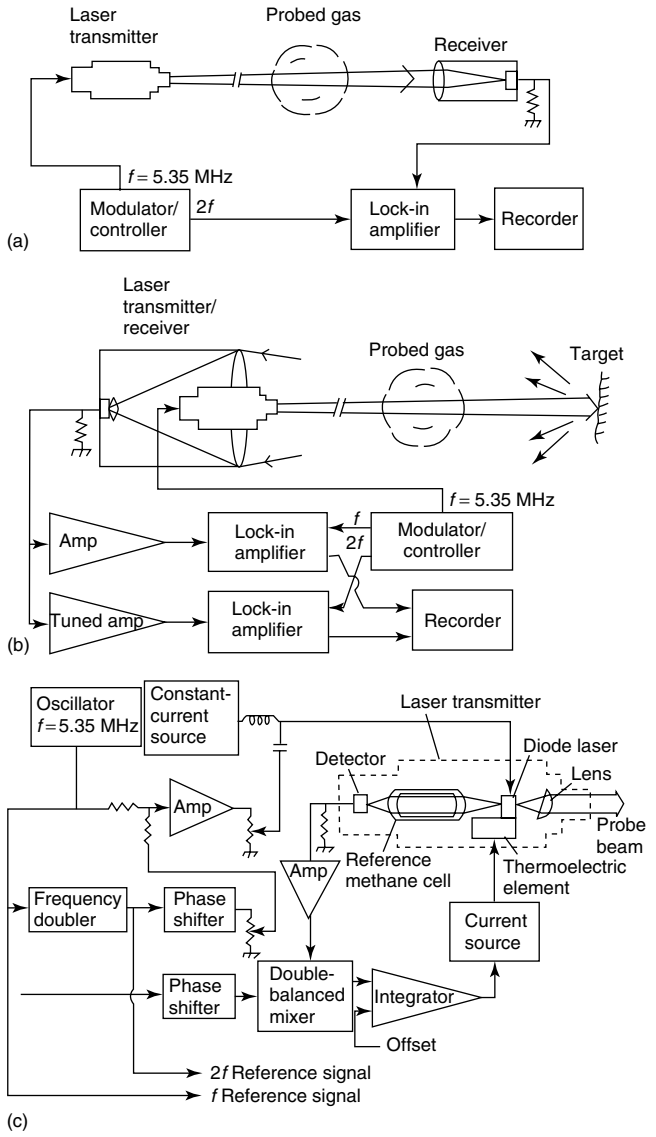

Figure 15 Diode laser methane sensor developed by Uehara and Tai,[21] in two remote detection schemes: (a) transmission and (b) reflection. (c) Schematics of the laser transmitter and its modulation controller. The transmitter housing is 4 cm in diameter.

Laser emission in this instrument was available from both front and rear facets of the laser chip and was detected using InGaAs pin photodiodes. The backward beam was used to dither-lock the laser wavelength to the center of the Q(6) line of methane in a reference cell. The 3-cm-long pyrex cell contained 200 torr of methane mixed with 560 torr of air. The cell windows functioned as lenses: one collimated the laser output, while the other focused it on to a reference detector. The laser injection current was modulated at a rate of $f = 5.35$ MHz, and the output of the reference detector was processed by a double-balanced mixer to recover the

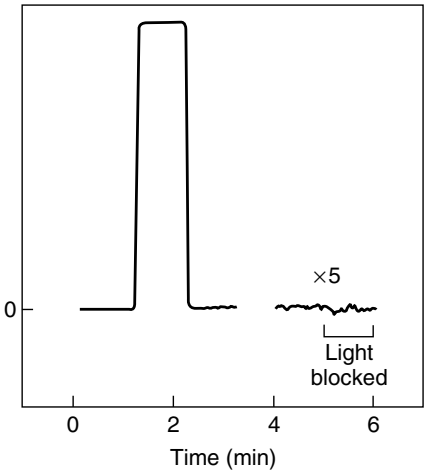

Figure 16 A $2f$ signal derived from a methane column density of 50 ppm m, lock-in-detected in the transmission scheme.[21] Inset on the right shows a $\times 5$ magnified noise. No background shift is observed when the laser beam is blocked.

amplitude of the first harmonic ($1f$) of the modulation frequency. Owing to AM–FM cross talk in the diode laser, the amplitude is nonzero even in the absence of absorption; therefore, offset cancellation was used to produce a suitable error signal. The error signal crosses zero when the laser frequency is scanned across the center of the absorption line and therefore can be used, after integration, as feedback to control the laser temperature. Such a simple locking scheme was reported to stabilize the center wavelength to within 10 MHz of the absorption line. After frequency stabilization was obtained, a small-amplitude second harmonic ($2f$) signal was added to the laser injection current to compensate the residual $2f$ signal amplitude in the detected *forward* laser beam in the absence of absorption. Absorption caused by the presence of methane in the signal beam path was then registered as a positive $2f$ amplitude.

Figure 16 shows an example of instrument output in the transmission scheme, in which the second harmonic amplitude alone was recorded. The signal was caused by a 100-ppm mixture of methane in air in a 50-cm-long cell. The mixture was introduced into the cell and purged subsequently with nitrogen, resulting in zero output after 2 min. The signal-to-noise ratio in the trace corresponds to a minimum detectable CH_4 column density of 0.3 ppm · m achieved using a signal averaging time of 1.3 s.

In the reflection detection scheme, the registered amplitude of the second harmonic depends not only on absorption but also on the range to the scattering target and on the target reflectance (wooden boards and concrete blocks were used). The amplitude of the first harmonic is directly proportional to the received optical power; quantitative detection was thus performed by computing a ratio of the $2f$ and $1f$

amplitudes. The corresponding detection sensitivity was 50 ppm · m. Although higher modulation frequencies are advantageous for noise reduction, caution must be exercised when they are used in the reflection scheme. When the beam path length from transmitter to receiver changes, the detected phases of the first and second harmonics also change. For a modulation frequency of 5.35 MHz, for example, a 3.5-m change in distance to target results in a 90° phase shift in the second harmonic signal. The phase shift must be tracked and compensated in order to maintain maximum signal intensity.[11,84,97,120,126–127]

5.2 Tunable Mid-infrared Diode Laser Absorption Spectrometer

In the area of MIR spectroscopy, the airborne tunable laser absorption spectrometer (ATLAS) developed by Podolske and Loewenstein[47] is an example of a self-contained field instrument. It was developed for *in situ* measurement of nitrous oxide and carbon monoxide in the lower stratosphere from an ER-2 high-altitude aircraft. Optical layout of the instrument is shown in Figure 17. A pressure-regulated liquid nitrogen Dewar-housed two different lead-salt lasers: one operating at 2169.2 cm^{-1} for the detection of carbon monoxide and another at 1270.2 cm^{-1} for the detection of nitrous oxide. After collimation by an off-axis parabolic mirror, the beam passed through an adjustable iris and the diagnostics section and was then partitioned into three beams (sample, reference, and zero) by organic pellicle beam splitters. These have the advantage of negligible thickness, hence beam displacement and small, 5–10%, amount of deflected light, so that most of the optical power remained in the sample beam. All three beams were measured by identical detectors. InAs detectors were used for the measurement of carbon monoxide at 4.7 μm, and HgCdTe detectors were used for the measurement of NO at 8 μm.

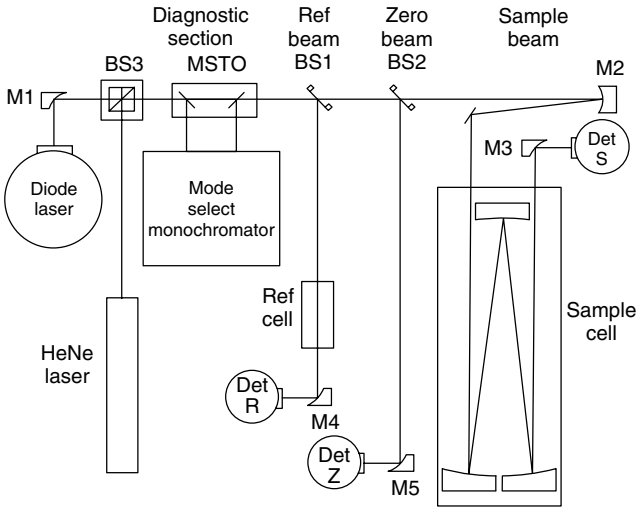

Figure 17 Optical layout of ATLAS by Podolske and Loewenstein.[47] The sample, reference, and zero beams are detected by detector S, R, and Z, respectively. The zero beam has the same optical path length as the sample beam external to the White cell. A bidirectional alignment beam is formed by a beam splitter BS3, illuminated by a HeNe laser. Mode-selecting monochromator and mode-selecting transfer optics are optional.

The instrument employed a noticeably complex laser current modulation and control scheme. Up to eight signals were superimposed to determine the instantaneous laser wavelength. Two of them were generated by an on-board computer for coarse and fine adjustments of the center wavelength. An adjustable amplitude, 2-kHz sine wave, was added to perform WM spectroscopy. The $1f$ feedback signal derived from the reference channel was also added for locking the laser wavelength to the center of a chosen absorption line (R(6) for carbon monoxide or P(17) for nitrous oxide). A 12.8-kHz triangle wave dither was also added to suppress the effective magnitude of optical interference fringes. Another signal, a 125-Hz triangle wave, was used to perform frequency scans for display purposes during the instrument set-up. For the measurement of dark detector output, each period of the waveform was preceded by a 125-μs pulse that gated off the laser injection current. Each gate pulse was immediately followed by another adjustable compensation pulse that provided heat to the laser junction that would have occurred in the absence of the gate pulse. The use of this compensation diminished the frequency drift associated with thermal recovery of the laser junction after each gate pulse.

In addition to optics, the ATLAS included a calibration and gas flow system (Figure 18). The gas flow system routed and conditioned the flow of both the reference gas (100 ppm CO in nitrogen or 1000 ppm N_2O in nitrogen)

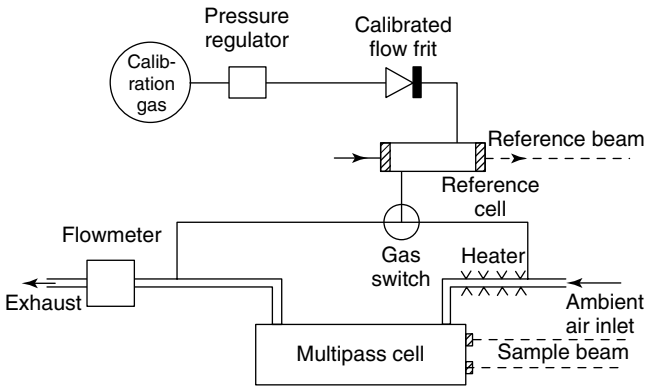

Figure 18 Diagram of the calibration and gas flow system of the ATLAS instrument.[47]

and the sample. Air was sampled from outside the aircraft boundary layer by means of a narrow inlet tube into which the air was propelled by ram pressure. The air then passed through a multipass cell with a residence time of approximately 1 s. Gas pressure and temperature inside the cell were maintained approximately equal to those of the reference cell. Pressure equalization was accomplished by a feedback-controlled flow of the reference gas through a frit, rather than by making it a static specimen. Gas temperatures were made equal by heating the incoming air to 25 °C; this also prevented temperature-induced alignment drift of the cell mirrors. For airborne measurements of nitrous oxide, whose typical abundance in air is approximately 300 ppb, the uncertainty of ±10% was estimated for ATLAS when using a signal averaging time of 1 s.

Apart from the systems described, the ATLAS had several electronic subsystems: laser control, analog signal processing, data acquisition, computer, and the pressure and temperature controls. To fully appreciate the complexity of an actual instrument designed for field applications, it is helpful to consult Fried et al.,[45,121] and Nelson et al.[120]

5.3 Gas Sensors Based on Difference-Frequency Generation Absorption Spectroscopy

As described in Section 3.4, difference-frequency mixing of NIR CW or pulsed-laser sources is another convenient technique to access the molecular 'fingerprint' region. Until recently, DFG sensors used discrete optical components to generate microwatt-level CW radiation.[68,85,122–124] More recently, the technologies developed for optical telecommunications – optical fiber and rare-earth-doped fiber amplifiers – have been used in DFG sensors. This approach has improved the robustness and reliability since it ensures permanent alignment of DFG pump channels without an increase in device complexity and cost. Lancaster et al.[65] built a portable sensor that is tunable from 3.25 to 4.4 μm (Figure 8).

A 20-mW ECDL with a tuning range of 814–870 nm and an Yb-doped fiber amplifier seeded by a 1083-nm DBR were mixed in a multigrating, temperature-controlled PPLN crystal. A 7.2-m-long fiber amplifier, pumped by a 2-W diode laser at 975 nm, produced 590-mW output power when seeded with 12 mW. All amplifier components were packaged into a $9 \times 11 \times 2\text{-cm}^3$ housing.

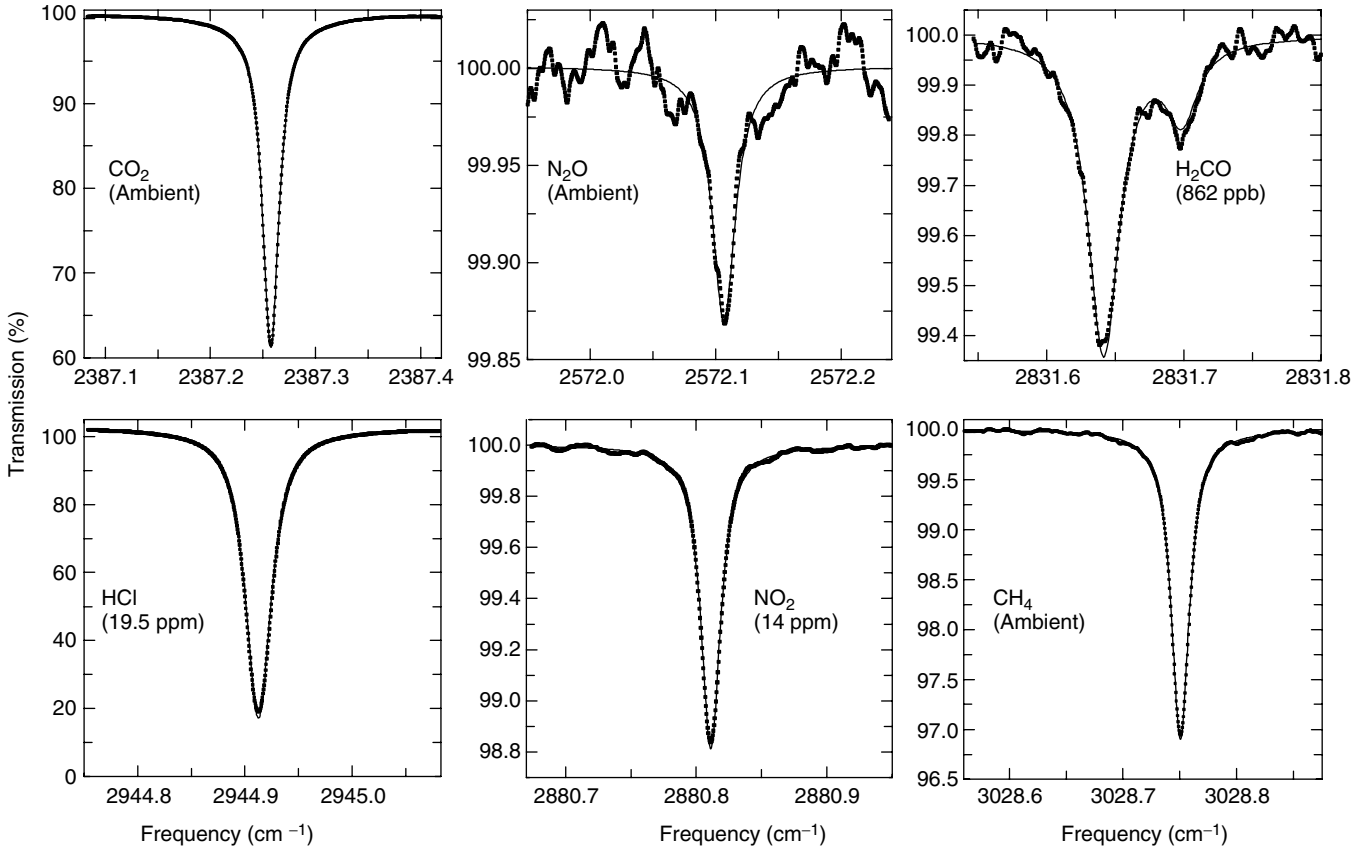

Figure 19 Detected absorption lines of several atmospheric trace gases.[65] (Reproduced from Ref. 65. © Springer, 1999.)

The pump wavelengths were combined by a low-loss fiber directional coupler. An $f = 1$ cm achromat lens was used for imaging the fiber output into the PPLN crystal. A 19-mm-long, 0.5-mm-thick crystal was used, with broadband antireflection coatings applied to both end faces. The crystal had eight domain grating periods, from 22.4 to 23.1 μm in 0.1-μm increments, and was temperature controlled in the 10–85 °C range. The DFG radiation is collimated by an $f = 5$ cm CaF_2 lens, and the residual pump light was blocked by a germanium filter. The radiation is either focused directly on a Peltier-cooled HgCdTe detector or aligned through a compact multipass cell with an effective path length from 18 to 100 m. The data acquisition system used was similar to the one used by Topfer et al.[68] and Lancaster et al.,[125] and consists of a compact 16-bit analog-to-digital converter card and a notebook computer. Detector voltage was sampled at a rate of 100 kHz and processed using a 9-kHz digital low-pass filter.

Coarse frequency tuning of the Littman-cavity ECDL (Figure 5) was performed by rotation of its tuning mirror with respect to the diffraction grating. The advantage of this configuration is a beam direction and a point of origin that are independent of wavelength; this allows stable coupling into an optical fiber. Fine tuning and repetitive frequency scans of up to 25 GHz were accomplished by linear current modulation of the seed DBR diode laser at a rate of 200 Hz. The instrument linewidth of 42 ± 5 MHz was measured indirectly by spectroscopy of methane at low pressure. Figure 19 shows the individual direct absorption spectra of six species of interest for trace-gas detection, which are within the 3.25- to 4.4-μm tuning range of the sensor, including CO_2, N_2O, H_2CO, HCl, NO_2, and CH_4. These spectra were taken at reduced pressure (88 torr) in a multipass cell using either calibrated gas mixtures or room air. Fitted Lorentzian lineshapes were used to determine gas concentrations. Stability of instrument performance was assessed by monitoring a methane line at 3028.751 cm^{-1} for an extended time period. In this experiment, a calibrated 1772.7 ± 1 ppb mixture of CH_4 in air was continuously flown through the multipass cell at a pressure of 88 torr. Observed standard deviation of the measurement was 0.8% (15 ppb).

The instrument occupies a 45×45-cm^2 optical breadboard mounted on a reinforced plastic suitcase for portability and weighs 25 kg. Total power consumption is approximately 60 W. To provide a continuous gas flow through the multipass cell at a controlled pressure, a two-stage diaphragm pump was used in series with a pressure flow controller. A capacitive manometer was used to measure the gas pressure just before using the multipass cell. For the measurement of reactive gases such as H_2CO, HCl, and NO_2, the gas handling system was maintained at 40 °C.

6 CONCLUSION

Spectroscopic sources for trace-gas monitoring, based on diode lasers, find increasing use in both established and new fields, including air-quality control; atmospheric chemistry; industrial, traffic, and agricultural emissions; chemical analysis, process control and medical diagnostics. The moderate cost, compact gas sensor using all-solid-state technology is capable of highly sensitive, selective detection and real-time analysis of a large number of gas species by means of absorption spectroscopy in the overtone and fundamental spectral regions. Reductions in cost and complexity, coupled with improved reliability and ease of operation, are now made as a result of the availability of several novel technologies developed by the telecommunications and computer industries that are equally applicable and useful in state-of-the-art gas sensors. Other recent technological breakthroughs, such as VCSELs, MEMS-VCSELs, QCLs (including EC-QCLs), and optical frequency combs (in NIR and MIR), to name a few, have started to find applications in trace-gas sensing and much more novel applications are certainly to come in a near future using these established or emerging technologies.

ACKNOWLEDGMENTS

The authors gratefully acknowledge stimulating input by a number of present and previous coworkers, graduate students and collaborators. This chapter also benefited from helpful suggestions and critical comments by Mark Allen of Physical Sciences, Inc. (Boston) and Adam Holyoake (John Wiley & Sons, Inc.).

ABBREVIATIONS AND ACRONYMS

AM	Amplitude Modulated
AMPM	Amplitude Modulated Phase Modulation
ATLAS	Airborne Tunable Laser Absorption Spectrometer
BRD	Balanced Ratiometric Detection
CRDS	Cavity Ring-down Spectroscopy
CW	Continuous Wave
DBR	Distributed Bragg Reflector
DFB	Distributed Feedback
DFG	Difference-frequency Generation
ECDL	External-cavity Diode Laser
EC-QCL	External-cavity Quantum Cascade Laser
FM	Frequency Modulation
FMS	Frequency Modulation Spectroscopy

KTP	Potassium Titanyl Phosphate
MDC	Minimal Detectable Concentration
MIR	Mid-infrared
NICE-OHMS	Noise-immune Cavity-enhanced Optical Heterodyne Molecular Spectroscopy
NIR	Near-infrared
OAS	Optoacoustic Spectroscopy
PA	Photoacoustic
PAS	Photoacoustic Spectroscopy
QCL	Quantum Cascade Laser
QTF	Quartz Tuning Fork
QEPAS	Quartz-enhanced Photoacoustic Spectroscopy
TTFM	Two-tone Frequency Modulation
TTFMS	Two-tone Frequency Modulation Spectroscopy
VCSEL	Vertical-cavity Surface-emitting Laser
WM	Wavelength Modulation
WMS	Wavelength Modulation Spectroscopy

RELATED ARTICLES

Environment: Trace Gas Monitoring **(Volume 3)**
Differential Optical Absorption Spectroscopy, Air Monitoring by • Environmental Trace Species Monitoring: Introduction • Fourier Transform Infrared Spectrometry in Atmospheric and Trace Gas Analysis • Infrared LIDAR Applications in Atmospheric Monitoring • Laser Absorption Spectroscopy, Air Monitoring by Tunable Mid-infrared Diode • Laser-based Combustion Diagnostics • Photoacoustic Spectroscopy in Trace Gas Monitoring • Cavity-Enhanced Spectroscopy: Applications, Theory and Instrumentation

REFERENCES

1. M.W. Sigrist (ed.), 'Air Monitoring by Spectroscopic Techniques', *Chemical Analysis*, John Wiley & Sons, Inc, New York, Vol. 27, 1994.
2. M.W. Sigrist, 'Air Monitoring, Optical Spectroscopic Methods', in *Encyclopedia of Environmental Analysis and Remediation*, ed. R.A. Meyers, John Wiley & Sons, Inc, New York, 84–117, 1998.
3. G. Gagliardi, L. Gianfrani, 'Trace-gas Analysis Using Diode Lasers in the Near-IR and Long-path Techniques', *Opt. Lasers Eng.*, **37**, 509–520 (2002).
4. J.A. Silver, A.C. Stanton, 'Optical Interference Fringe Reduction in Laser-absorption Experiments', *Appl. Opt.*, **27**, 1914–1916 (1988).
5. J. Reid, M. El-Sherbiny, B.K. Garside, E.A. Ballik, 'Sensitivity Limits of a Tunable Diode Laser Spectrometer with Application to the Detection of NO_2 at the 100-ppt Level', *Appl. Opt.* **19**, 3349–3354 (1980).
6. H.I. Schiff, G.I. Mackay, J. Bechara, 'The Use of Tunable Diode Laser Absorption Spectroscopy for Atmospheric Measurements', in *Air Monitoring by Spectroscopic, Techniques*, ed. M.W. Sigrist, Wiley, New York, 1994, Chapter 5.
7. P. Werle, 'Accuracy and Precision of Laser Spectrometers for Trace Gas Sensing in the Presence of Optical Fringes and Atmospheric Turbulence', *Appl. Phys. B*, **102**(2), 313–329 (2011).
8. A.G. Maki, J.S. Wells, *Wavenumber Calibration Tables from Heterodyne Frequency Measurements*, Spec. Publ. 821 National Institute of Standards and Technology, Gaithersburg, MD, 1991.
9. L.S. Rothman, I.E. Gordon, A. Barbe, D.C. Benner, P.F. Bernath, M. Birk, V. Boudon, L.R. Brown, A. Campargue, J.-P. Champion, K. Chance, L.H. Coudert, V. Dana, V.M. Devi, S. Fally, J.-M. Flaud, R.R. Gamache, A. Goldman, D. Jacquemart, I. Kleiner, N. Lacome, W.J. Lafferty, J.-Y. Mandin, S.T. Massie, S.N. Mikhailenko, C.E. Miller, N. Moazzen-Ahmadi, O.V. Naumenko, A.V. Nikitin, J. Orphal, V.I. Perevalov, A. Perrin, A. Predoi-Cross, C.P. Rinsland, M. Rotger, M. Šimečková, M.A.H. Smith, K. Sung, S.A. Tashkun, J. Tennyson, R.A. Toth, A.C. Vandaele, J. Vander Auwera, 'The HITRAN 2008 Molecular Spectroscopic Database', *J. Quant. Spectrosc. Radiat. Transf.*, **110**, 533–572 (2009).
10. N. Jacquinet-Husson, L. Crepeau, R. Armante, C. Boutammine, A. Chédin, N.A. Scott, C. Crevoisier, V. Capelle, C. Boone, N. Poulet-Crovisier, A. Barbe, A. Campargue, D. Chris Benner, Y. Benilan, B. Bézard, V. Boudon, L.R. Brown, L.H. Coudert, A. Coustenis, V. Dana, V.M. Devi, S. Fally, A. Fayt, J.-M Flaud, A. Goldman, M. Herman, G.J. Harris, D. Jacquemart, A. Jolly, I. Kleiner, A. Kleinböhl, F. Kwabia-Tchana, N. Lavrentieva, N. Lacome, L.-H. Xu, O.M. Lyulin, J.-Y. Mandin, A. Maki, S. Mikhailenko, C.E. Miller, T. Mishina, N. Moazzen-Ahmadi, H.S.P. Müller, A. Nikitin, J. Orphal, V. Perevalov, A. Perrin, D.T. Petkie, A. Predoi-Cross, C.P. Rinsland, J.J. Remedios, M. Rotger, M.A.H Smith, K. Sung, S. Tashkun, J. Tennyson, R.A. Toth, A.-C. Vandaele, J. Vander Auwera, 'The 2009 Edition of the GEISA Spectroscopic Database', *J. Quant. Spectrosc. Radiat. Transf.* (2011). DOI: 10.1016/j.jqsrt.2011.06.004.
11. R.M. Mihalcea, M.E. Webber, D.S. Baer, R.K. Hanson, G.S. Feller, W.B. Chapman, 'Diode-laser Absorption Measurements of CO_2, H_2O, N_2O, and NH_3 Near 2.0 μm', *Appl. Phys. B*, **67**(3), 283–288 (1998).
12. D.M. Sonnenfroh, M.G. Allen, 'Observation of CO and CO_2 Absorption Near 1.57 μm with an External-cavity Diode Laser', *Appl. Opt.*, **36**(15), 3298–3300 (1997).

13. Norsk Elektro Optikk, *Laser Gas Monitors, Technical Description*, Norway, 1996.
14. Southwest Sciences Inc., *Detection Limits*, http://www.iac.net/~dchovde/.
15. Bovar–Western Research, *Spectrascan: Technical Specifications*, Ref. No. 908-0001 Rev. 0.
16. M.G. Allen, K.L. Carleton, S.J. Davis, W.J. Kessler, C.E. Otis, D.A. Palombo, D.M. Sonnenfroh, 'Ultrasensitive Dual-beam Absorption and Gain Spectroscopy: Applications for Near-infrared and Visible Diode Laser Sensors', *Appl. Opt.*, **34**(18), 3240–3249 (1995).
17. M. Fehér, P.A. Martin, A. Rohrbacher, A.M. Soliva, J.P. Maier, 'Inexpensive Near-Infrared Diode-laser-based Detection System for Ammonia', *Appl. Opt.*, **32**(12), 2028–2030 (1993).
18. J. Humlicek, 'An Efficient Method for Evaluation of the Complex Probability Function: The Voigt Function and its Derivatives', *J. Quant. Spectrosc. Radiat. Transfer*, **21**, 309 (1979).
19. A. Lytkine, W. Jäger, J. Tulip, 'Frequency Tuning of Long-wavelength VCSELs', *Spectrochim. Acta, Part A*, **63**, 940–946 (2006).
20. C.E. Wieman, L. Hollberg, 'Using Diode Lasers for Atomic Physics', *Rev. Sci. Instrum.*, **62**, 1 (1991).
21. K. Uehara, H. Tai, 'Remote Detection of Methane with a 1.66 μm Diode Laser', *Appl. Opt.*, **31**, 809 (1992).
22. H. Tai, K. Yamamoto, M. Uchida, S. Osawa, K. Uehara, 'Long Distance Simultaneous Detection of Methane and Acetylene by Using Diode Lasers Coupled with Optical Fibers', *IEEE Photon. Technol. Lett.*, **4**, 804 (1992).
23. M. Lackner, G. Totschnig, F.W. Winter, M. Ortsiefer, M.-C. Amann, R. Shau, J. Rosskopf, 'Demonstration of Methane Spectroscopy Using a Vertical-cavity Surface-emitting Laser at 1.68 μm with up to 5 MHz Repetition Rate', *Meas. Sci. Technol.*, **14**, 101–106 (2003).
24. G. Totschnig, M. Lackner, R. Shau, M. Ortsiefer, J. Rosskopf, M.-C. Amann, F. Winter, '1.8 μm Vertical-cavity Surface-emitting Laser Absorption Measurements of HCl, H_2O and CH_4', *Meas. Sci. Technol.*, **14**, 472–478 (2003).
25. M. Laakso, M. Jalonen, S. Laukkanen, 'A Compact Ruggedized Tunable Diode Laser Spectrometer for Oxygen Sensing', *Proceedings of ISA Expo 2005*, Chicago, USA, 25–27 October 2005.
26. S.J. Chen, J.A. Silver, Detection of Explosive Mixtures in the Ullage of Aircraft Fuel Tanks, *42nd AIAA Aerospace Sciences Meeting and Exhibit*, Reno, Nevada, 5–8 January 2004.
27. J. Chen, A. Hangauer, R. Strzoda, M.-C. Amman, 'Laser Spectroscopic Oxygen Sensor Using Diffuse Reflector Based Optical Cell and Advanced Signal Processing', *Appl. Phys. B*, **100**, 417–425 (2010).
28. D.C. Hovde, C.A. Parsons, 'Wavelength Modulation Detection of Water Vapor with a Vertical Cavity Surface-emitting Laser', *Appl. Opt.*, **36**, 1135–1138 (1997).
29. G. Totschnig, M. Lackner, R. Shau, M. Ortsiefer, J. Rosskopf, M.-C. Amann, F. Winter, 'High-speed Vertical-cavity Surface-emitting Laser (VCSEL) Absorption Spectroscopy of Ammonia (NH_3) Near 1.54 μm', *Appl. Phys. B*, **76**, 603–608 (2003).
30. P. Ortwein, W. Woiwode, S. Wagner, M. Gisi, V. Ebert, 'Laser-based Measurements of Line Strength, Self- and Pressure-broadening Coefficients of the $H^{35}Cl$ R(3) Absorption Line in the First Overtone Region for Pressures up to 1 MPa', *Appl. Phys. B*, **100**, 341–347 (2010).
31. J. Chen, A. Hangauer, R. Strzoda, M.-C. Amann, 'VCSEL-based Calibration-free Carbon Monoxide Sensor at 2.3 μm with In-line Reference Cell', *Appl. Phys. B*, **102**(2), 381–389 (2011).
32. A. Lytkine, W. Jäger, J. Tulip, 'Tunable Diode Laser Spectroscopy of Ethylene Oxide Near 1693 nm', *Appl. Phys. B*, **98**, 871–876 (2010).
33. M. Lackner, M. Schwarzott, F. Winter, B. Kögel, S. Jatta, H. Halbritter, P. Meissner, 'CO and CO_2 Spectroscopy Using a 60 nm Broadband Tunable MEMS-VCSEL at ~1.55 μm', *Opt. Lett.* **31**(21), 3170–3172 (2006).
34. B. Kögel, H. Halbritter, S. Jatta, M. Maute, G. Böhm, M.-C. Amann, M. Lackner, M. Schwarzott, F. Winter, P. Meissner, 'Simultaneous Spectroscopy of NH_3 and CO Using a >50 nm Continuously Tunable MEMS-VCSEL', *IEEE Sens. J.*, **7**(11), 1483–1489 (2007).
35. S. Schilt, K. Zogal, B. Kögel, P. Meissner, M. Maute, R. Protasio, M.-C. Amann, 'Spectral and Modulation Properties of a Largely Tunable MEMS-VCSEL in View of Gas Phase Spectroscopy Applications', *Appl. Phys. B*, **100**(2), 321–329 (2010).
36. A.T. Schremer, C.L. Tang, 'External-cavity Semiconductor Laser with 1000 GHz Continuous Piezoelectric Tuning Range', *IEEE Photonics Technol. Lett.*, **2**(1), 3–5 (1990).
37. D.B. Oh, D.C. Hovde, 'Wavelength-modulation Detection of Acetylene with Near-infrared External Cavity Diode Laser', *Appl. Opt.*, **34**, 7002 (1995).
38. T.W. Hänsch, 'Nobel Lecture: Passion for Precision', *Rev. Mod. Phys.*, **78**, 1297–1309 (2006).
39. M.C. Stowe, M.J. Thorpe, A. Pe'er, J. Ye, J.E. Stalnaker, V. Gerginov, S.A. Diddams, 'Direct Frequency Comb Spectroscopy', *Adv. At. Mol. Opt. Phys.*, **55**, 1–60 (2008).
40. S.A. Diddams, L. Hollberg, V. Mbele, 'Molecular Fingerprinting with the Resolved Modes of a Femtosecond Laser Frequency Comb', *Nature*, **445**, 627–630 (2007).
41. M.J. Thorpe, K.D. Moll, R.J. Jones, B. Safdi, J. Ye, 'Broadband Cavity Ringdown Spectroscopy for Sensitive

and Rapid Molecular Detection', *Science*, **311**, 1595–1599 (2006).

42. Z. Feit, D. Kostyk, R.J. Woods, P. Mak, 'Molecular Beam Epitaxy Grown PbEuSeTe Buried-heterostructure Lasers with Continuous Wave Operation @ 195 K', *Appl. Phys. Lett.*, **57**, 2891 (1990).
43. H.I. Schiff, D.R. Karecki, G.W. Harris, D.R. Hastie, G.I. Mackay, 'A Tunable Diode Laser System for Aircraft Measurements of Trace Gas', *J. Geophys. Res.*, **95**, 10147–10153 (1990).
44. P. Werle, R. Mücke, F. Slemr, 'The Limits of Signal Averaging in Atmospheric Trace-gas Monitoring by Tunable Diode-laser Absorption Spectroscopy (TDLAS)', *Appl. Phys. B*, **57**(2), 131–139 (1993).
45. A. Fried, S. McKeen, S. Sewell, J. Harder, B. Henry, P. Golden, 'Photochemistry of Formaldehyde During the 1993 Tropospheric OH Photochemistry Experiment', *J. Geophys. Res.*, **102**, 6283 (1997).
46. C.R. Webster, R.D. May, 'Simultaneous *In situ* Measurements and Diurnal Variations of NO, NO_2, O_3, NO_2, CH_4, H_2O, and CO_2 in the 40 – 26-km Region Using an Open Path Tunable Diode Laser Spectrometer', *J. Geophys. Res.*, **92**, 11 931 (1987).
47. J. Podolske, M. Loewenstein, 'Airborne Tunable Diode Laser Spectrometer for Trace Gas Measurement in the Lower Stratosphere', *Appl. Opt.*, **32**, 5324 (1993).
48. J. Faist, F. Capasso, D.L. Sivco, C. Sirtori, A.L. Hutchinson, A.Y. Cho, 'Quantum Cascade Lasers', *Science*, **264**, 553–556 (1994).
49. O. Cathabard, R. Teissier, J. Devenson, A.N. Baranov, 'InAs-based Distributed Feedback Quantum Cascade Lasers', *Electron. Lett.*, **45**, 1028–1029 (2009).
50. M. Beck, D. Hofstetter, T. Aellen, J. Faist, U. Oesterle, M. Illegems, E. Gini, H. Melchior, 'Continuous Wave Operation of a Mid-infrared Semiconductor Laser at Room Temeprature', *Sciences*, **295**, 301–303 (2002).
51. J. Faist, C. Gmachl, F. Capasso, C. Sirtori, D.L. Silvco, J.N. Baillargeon, A.Y. Cho, 'Distributed Feedback Quantum Cascade Lasers', *Appl. Phys. Lett.*, **70**(20), 2670–2672 (1997).
52. R. Maulini, M. Beck, J. Faist, E. Gini, 'Broadband Tuning of External Cavity Bound-to-continuum Quantum-cascade Lasers', *Appl. Phys. Lett.*, **84**(10), 1659–1661 (2004).
53. R. Lewicki, G. Wysocki, A.A. Kosterev, F.K. Tittel, 'QEPAS Based Detection of Broadband Absorbing Molecules Using a Widely Tunable, CW Quantum Cascade Laser at 8.4 μm', *Opt. Express*, **15**(12), 7357–7366 (2007).
54. A. Mukherjee, M. Prasanna, M. Lane, R. Go, I. Dunayevskiy, A. Tsekoun, C.K.N. Patel, 'Optically Multiplexed Multi-gas Detection Using Quantum Cascade Laser Photoacoustic Spectroscopy', *Appl. Opt.*, **47**(27), 4884–4887 (2008).
55. D.D. Nelson, B. McManus, S. Urbanski, S. Herndon, M.S. Zahniser, 'High Precision Measurements of Atmospheric Nitrous Oxide and Methane Using Thermoelectrically Cooled Mid-infrared Quantum Cascade Lasers and Detectors', *Spectrochim. Acta, Part A*, **60**, 3325–3335 (2004).
56. D.M. Sonnenfroh, W.T. Rawlins, M.G. Allen, C. Gmachl, F. Capasso, A.L. Hutchinson, D.L. Sivco, J.N. Baillargeon, A.Y. Cho, 'Application of Balanced Detection to Absorption Measurements of Trace Gases with Room-temperature, Quasi-cw Quantum-cascade Lasers', *Appl. Opt.*, **40**(6), 812–820 (2001).
57. K. Namjou, S. Cai, E.A. Whittaker, J. Faist, C. Gmachl, F. Capasso, D.L. Sivco, A.Y. Cho, 'Sensitive Absorption Spectroscopy with a Room-temperature Distributed-feedback Quantum-cascade Laser', *Opt. Lett.*, **23**(3), 219–221 (1998).
58. S. Borri, S. Bartalini, P. De Natale, M. Inguscio, C. Gmachl, F. Capasso, D.L. Sivco, A.Y. Cho, 'Frequency Modulation Spectroscopy by Means of Quantum-cascade Lasers', *Appl. Phys. B*, **85**(2–3), 223–229 (2006).
59. B.A. Paldus, T.G. Spence, R.N. Zare, J. Oomens, F.J.M. Harren, D.H. Parker, C. Gmachl, F. Capasso, D.L. Sivco, J.N. Baillargeon, A.L. Hutchinson, A.Y. Cho, 'Photoacoustic Spectroscopy Using Quantum-cascade Lasers', *Opt. Lett.*, **24**(3), 178–180 (1999).
60. B.A. Paldus, C.C. Harb, T.G. Spence, R.N. Zare, C. Gmachl, F. Capasso, D.L. Sivco, J.N. Baillargeon, A.L. Hutchinson, A.Y. Cho, 'Cavity Ringdown Spectroscopy Using Mid-infrared Quantum-cascade Lasers', *Opt. Lett.*, **25**(9), 666–668 (2000).
61. M.T. McCulloch, N. Langford, G. Duxbury, 'Real-time Trace-level Detection of Carbon Dioxide and Ethylene in Car Exhaust Gases', *Appl. Opt.*, **44**(14), 2887–2894 (2005).
62. K.P. Petrov, S. Waltman, U. Simon, R.F. Curl, F.K. Tittel, E.J. Dlugokencky, L. Hollberg, 'Detection of Methane in Air Using Diode-laser Pumped Difference Frequency Generation Near 3.2 μm', *Appl. Phys. B*, **61**, 553 (1995).
63. A. Pine, 'Doppler-limited Molecular Spectroscopy by Difference-frequency Mixing', *J. Opt. Soc. Am.*, **64**(12), 1683–1690 (1974).
64. U. Simon, C.E. Miller, C.C. Bradley, R.G. Hulet, R.F. Curl, F.K. Tittel, 'Difference Frequency Generation in $AgGaS_2$ by Use of Single Mode Diode Laser Pump Sources', *Opt. Lett.*, **18**, 1062 (1993).
65. D.G. Lancaster, D. Richter, F.K. Tittel, 'Portable Fiber-coupled Diode-laser-based Sensor for Multiple Trace Gas Detection', *Appl. Phys. B*, **69**(5–6), 459–465 (1999).

66. G. Rosenman, Kh. Garb, A. Skliar, M. Oron, D. Eger, M. Katz, 'Domain Broadening in Quasi-phase Matched Nonlinear Optical Devices', *Appl. Phys. Lett.*, **73**, 865 (1998).

67. L.E. Myers, W.R. Bosenberg, 'Periodically Poled Lithium Niobate and Quasi-phase-matched Optical Parametric Oscillators', *IEEE J. Quant. Electron.*, **33**, 1663 (1997).

68. T. Topfer, K.P. Petrov, Y. Mine, D. Jundt, R.F. Curl, F.K. Tittel, 'Room Temperature Mid-infrared Laser Sensor for Trace Gas Detection', *Appl. Opt.*, **36**, 8042 (1997).

69. G.D. Boyd, D.A. Kleinman, 'Parametric Interaction of Focused Gaussian Light Beams', *J. Appl. Phys.*, **39**, 3597–3639 (1968).

70. T.-B. -Chu, M. Broyer, 'Intracavity cw Difference Frequency Generation by Mixing Three Photons and Using Gaussian Laser Beams', *J. Phys. France*, **46**(4), 523–533 (1985).

71. L. Goldberg, W.K. Burns, R.W. McElhanon, 'Difference Frequency Generation of Tunable Mid-infrared Radiation in Bulk Periodically Poled $LiNbO_3$', *Opt. Lett.*, **20**, 1280 (1995).

72. M.L. Bortz, M.A. Arbore, M.M. Fejer, 'Quasi-phase Matched Optical Parametric Amplification and Oscillation in Periodically Poled $LiNbO_3$ Waveguides', *Opt. Lett.*, **20**, 49 (1994).

73. J. Webjorn, F. Laurell, G. Arvidsson, 'Fabrication of Periodically Domain-inverted Channel Waveguides in Lithium Niobate for Second Harmonic Generation', *J. Lightwave Technol.*, **7**, 1597–1600 (1989).

74. C.E. Rice, 'The structure and Properties of $Li_{1-x}H_xNbO_3$', *J. Solid State Chem.*, **64**(2), 188–199 (1986).

75. M.H. Chou, M.A. Arbore, M.M. Fejer, 'Adiabatically Tapered Periodic Segmentation of Channel Waveguides for Node-size Transformation and Fundamental Mode Excitation', *Opt. Lett.*, **21**, 794 (1996).

76. M.H. Chou, J. Hauden, M.A. Arbore, M.M. Fejer, '1.5-μm Band Wavelength Conversion Based on Difference Frequency Generation in $LiNbO_3$ Waveguides with Integrated Coupling Structures', *Opt. Lett.*, **23**, 1004 (1998).

77. K.P. Petrov, A.T. Ryan, T.L. Patterson, L. Huang, S.J. Field, D.J. Bamford, 'Mid-infrared Spectroscopic Detection of Trace Gases Using Guided-wave-difference-frequency Generation', *Appl. Phys. B*, **67**, 357 (1998).

78. H. Wächter, M.W. Sigrist, 'Generation of Coherent Mid-infrared Radiation by Difference Frequency Mixing', in *Springer Handbook of Lasers and Optics, Chapter 11.10: Lasers and Coherent Sources*, ed. F. Träger, Springer, Berlin, Heidelberg 801–814, Chapter 11.10, 2007.

79. C. Fischer, M.W. Sigrist, 'Mid-IR Difference Frequency Generation', in *Solid-State Mid-Infrared Laser Sources*, eds. I.T. Sorokina, K.L. Vodopyanov, Springer, *Topics in Applied Physics*, 97–140, Vol. 89, 2003.

80. P. Maddaloni, P. Malara, G. Gagliardi, P. De Natale, 'Mid-infrared Fibre-based Optical Comb', *New J. Phys.*, **8**, 1–8 (2006).

81. S.M. Foreman, A. Marian, J. Ye, E.A. Petrukhin, M.A. Gubin, O.D. Mueck, F.N.C. Wong, R.P. Ippen, F.X. Kaertner, 'Demonstration of a HeNe/CH_4-based Optical Molecular Clock', *Opt. Lett.*, **30**, 570–572 (2006).

82. W.B. Grant, R.H. Kagann, W.A. McClenny, 'Optical Remote Measurement of Toxic Gases', *J. Air Waste Manag. Assoc.*, **42**(1), 18–30 (1992).

83. J.B. McManus, P.L. Kebabian, M.S. Zahniser, 'Astigmatic Mirror Multipass Absorption Cells for Long-path Length Spectroscopy', *Appl. Opt.*, **34**, 3336 (1995).

84. K.P. Petrov, R.F. Curl, F.K. Tittel, 'Compact Laser Difference Frequency Spectrometer for Multi-component Trace Gas Detection', *Appl. Phys. B*, **66**, 531 (1998).

85. K. Nakagawa, T. Katsuda, A.S. Shelkovnikov, M. de Labachelerie, M. Ohtsu, 'Highly Sensitive Detection of Molecular Absorption Using a High Finesse Optical Cavity', *Opt. Commun.*, **107**, 369 (1994).

86. G. Meijer, M.G.H. Boogaarts, R.T. Jongma, D.H. Parker, A.M. Wodtke, 'Coherent Cavity Ring Down Spectroscopy', *Chem. Phys. Lett.*, **217**, 112 (1994).

87. G. Meijer, M.G.H. Boogaarts, R.T. Jongma, D.H. Parker, A.M. Wodtke, 'Cavity Enhanced Absorption and Cavity Enhanced Magnetic Rotation Spectroscopy', *Rev. Sci. Instrum.*, **69**, 3763 (1998).

88. J.J. Scherer, J.B. Paul, C.P. Collier, A. O'Keefe, D.J. Rakestraw, R.J. Saykally, 'Cavity Ringdown Laser Spectroscopy: A New Ultrasensitive Absorption Technique', *Spectroscopy*, **11**(5), 46–50 (1996).

89. R.A. Provencal, J.B. Paul, C.N. Chapo, R.J. Saykally, 'Cavity Ringdown Laser Absorption Spectroscopy', *Spectroscopy*, **14**(4), 24 (1999).

90. G. Berden, R. Engeln (eds), *Cavity Ring Down Spectroscopy: Techniques and Applications*, John Wiley & Sons, Inc, 2009.

91. C.J. Young, R.A. Washenfelder, S.S. Brown, 'Cavity Enhanced Spectroscopy: Applications Theory and Instrumentation', in *Encyclopedia of Analytical Chemistry*, ed. R.A. Meyers, John Wiley, Chichester, 2011. DOI: 10.1002/9780470027318.a9195.

92. T.G. Spence, C.C. Harb, B.A. Paldus, R.N. Zare, B. Willke, R.L. Byer, 'A Laser-locked Cavity Ring-down Spectrometer Employing an Analog Detection Scheme', *Rev. Sci. Instrum.*, **71**, 347–354 (2000).

93. S. Tranchart, I.H. Bachir, J.-L. Destombes, 'Sensitive Trace Gas Detection with Near Infrared Laser Diodes and an Integrating Sphere', *Appl. Opt.*, **35**, 7070 (1996).

94. J. Masiyano, J. Hodgkinson, R.P. Tatam, 'Gas Cells for Tunable Diode Laser Absorption Spectroscopy Employing Optical Diffusers. Part 2: Integrating Spheres', *Appl. Phys. B*, **100**, 303–312 (2010).

95. P.C.D. Hobbs, IBM Corp, Armonk, N.Y., Noise Canceling Circuitry for Optical Systems with Signal Dividing and Combining Means, US Patent No. 5,134,276, July 28, 1992.

96. P. Werle, 'A Review of Recent Advances in Semiconductor Laser Based Gas Monitors', *Spectrochim. Acta, Part A*, **54**, 197–236 (1998).

97. G.C. Bjorklund, 'Frequency-modulation Spectroscopy: A New Method for Measuring Weak Absorption and Dispersions', *Opt. Lett.*, **5**, 15 (1980).

98. D.E. Cooper, T.F. Gallagher, 'Double Frequency Modulation Spectroscopy: High Modulation Frequency with Low-bandwidth Detectors', *Appl. Opt.*, **24**, 1327 (1985).

99. R. Großkloß, P. Kersten, W. Demtröder, 'Sensitive Amplitude- and Phase-modulated Absorption- spectroscopy with a Continuously Tunable Diode Laser', *Appl. Phys. B*, **58**, 137 (1994).

100. J. Ye, L.-S. Ma, J.L. Hall, 'Ultrasensitive Detections in Atomic and Molecular Physics: Demonstration in Molecular Overtone Spectroscopy', *J. Opt. Soc. Am. B*, **15**(1), 6–15 (1998).

101. A. Foltynowicz, F.M. Schmidt, W. Ma, O. Axner, 'Noise-immune Cavity-enhanced Optical Heterodyne Molecular Spectroscopy: Current Status and Future Potential', *Appl. Phys. B*, **92**, 313–326 (2008).

102. M.S. Taubman, T.L. Myers, B.D. Cannon, R.M. Williams, 'Stabilization, Injection and Control of Quantum Cascade Lasers, and their Application to Chemical Sensing in the Infrared', *Spectrochim. Acta, Part A*, **60**(14), 3457–3468 (2004).

103. F.S. Pavone, M. Inguscio, 'Frequency and Wavelength Modulation Spectroscopies: Comparison of Experimental Methods Using an AlGaAs Diode Laser', *Appl. Phys. B*, **56**, 118 (1993).

104. A.N. Dharamsi, A.M. Bullock, 'Applications of Wavelength-modulation Spectroscopy in Resolution of Pressure and Modulation Broadened Spectra', *Appl. Phys. B*, **63**, 283–292 (1996).

105. A.A. Kosterev, F.K. Tittel, D.V. Serebryakov, A.L. Malinovski, I.V. Morozov, 'Applications of Quartz Tuning Forks in Spectroscopic Gas Sensing', *Rev. Sci. Instrum.*, **76**, 043105 (2005).

106. M.W. Sigrist, 'Air Monitoring by Laser Photoacoustic Spectrosopy', in *Air Monitoring by Spectroscopic Techniques*, *Chemical Analysis Series*, ed. M.W. Sigrist, Wiley, New York, Vol. 127, Chapter 4, 1994.

107. M.W. Sigrist, S. Bernegger, P.L. Meyer, 'Atmospheric Pollution Monitoring Using CO_2 Laser Photoacoustic Spectroscopy and Other Techniques', *Rev. Sci. Instrum.*, **61**, 1779 (1990).

108. M. Fehér, Y. Jiang, J.P. Maier, A. Miklós, 'Optoaccoustic Trace-gas Monitoring with Near Infrared Diode Lasers', *Appl. Opt.*, **33**, 1655 (1994).

109. S. Bernegger, CO-laser Photoacoustic Spectroscopy of Gases and Vapors for Trace Gas Analysis, Diss. ETH N° 8636, 1988.

110. S. Schilt, J.-P. Besson, L. Thévenaz, 'Near-infrared Laser Photoacoustic Detection of Methane: The Impact of Molecular Relaxation', *Appl. Phys. B*, **82**(2), 319–328 (2006).

111. A. Veres, Z. Bozoki, A. Mohacsi, M. Szakall, G. Szabo, 'External Cavity Diode Laser Based Photoacoustic Detection of CO_2 at 1.43 μm: The Effect of Molecular Relaxation', *Appl. Spectrosc.*, **57**(8), 900–905 (2003).

112. L.B. Kreuzer, 'Signal Generation and Detection', in *Optoacoustic Spectroscopy and Detection*, ed. Y.-H. Pao, Academic Press, New York, 1–25, 1977, Chapter 1.

113. C.F. Dewey, 'Design of Optoacoustic Systems', in *Optoacoustic Spectroscopy and Detection*, ed. Y.-H. Pao, Academic Press, New York, 47–77, 1977, Chapter 3.

114. R. Bartlome, M. Kaucikas, M.W. Sigrist, 'Modulated Resonant Versus Pulsed Resonant Photoacoustics in Trace Gas Detection', *Appl. Phys. B*, **96**, 561–566 (2009).

115. S. Schilt, L. Thévenaz, M. Niklés, L. Emmenegger, C. Hüglin, 'Ammonia Monitoring at Trace Level Using Photoacoustic Spectroscopy in Industrial and Environmental Applications', *Spectrochim. Acta, Part A*, **60**, 3259–3268 (2004).

116. G. Wysocki, A.A. Kosterev, F.K. Tittel, 'Influence of Molecular Relaxation Dynamics on Quartz-enhanced Photoacoustic Detection of CO_2 at $\lambda = 2\,\mu m$', *Appl. Phys. B*, **85**, 301–306 (2006).

117. A. Miklós, Z. Bozóki, Y. Jiang, M. Fehér, 'Experimental and Theoretical Investigation of Photoacoustic Signal Generation by Wavelength Modulated Diode Lasers', *Appl. Phys. B*, **58**, 483 (1994).

118. S. Schilt, L. Thévenaz, 'Wavelength Modulation Photoacoustic Spectroscopy: Theoretical Description and Experimental Results', *Infrared Phys. Technol.*, **48**(2), 154–162 (2006).

119 D.M. Sonnenfroh, W.J. Kessler, J.C. Magill, B.L. Upschulte, M.G. Allen, J.D.W. Barrick, 'In-situ Sensing of Tropospheric Water Vapor Using an Airborne Near Infrared Diode Laser Hygrometer', *Appl. Phys. B*, **67**, 275 (1998).

120. D.D. Nelson, M.S. Zahniser, J.B. McManus, C.E. Kolb, J.L. Jimenez, 'A Tunable Diode Laser System for the

Remote Sensitive of On-road Vehicle Emissions', *Appl. Phys. B*, **67**, 433 (1998).

121. A. Fried, B. Henry, B. Wert, S. Sewell, J.R. Drummond, 'Laboratory, Ground-based, and Airborne Tunable Diode Laser Systems: Performance Characteristics and Applications in Atmospheric Studies', *Appl. Phys. B*, **67**, 317 (1998).

122. M. Seiter, D. Keller, M.W. Sigrist, 'Broadly Tunable Difference-frequency Spectrometer for Trace Gas Detection with Nonlinear Critical Phase-matching in $LiNbO_3$', *Appl. Phys. B*, **67**, 351 (1998).

123. B. Sumpf, D. Rehle, T. Kelz, H.-D. Kronfeldt, 'A Tunable Diode-laser Spectrometer for the MIR Region Near 7.2 μm Applying Difference Frequency Generation in $AgGaSe_2$', *Appl. Phys. B*, **67**, 369 (1998).

124. W. Chen, G. Mouret, D. Boucher, 'Difference-frequency Laser Spectroscopy Detection of Acetylene Trace Constituent', *Appl. Phys. B*, **67**, 375 (1998).

125. D.G. Lancaster, D. Richter, R.F. Curl, F.K. Tittel, 'Real-time Measurements of Trace Gas Using a Compact Difference Frequency Based Sensor Operation at 3.5 μm', *Appl. Phys. B*, **67**, 339 (1998).

126. G. Modugno, C. Corsi, M. Gabrysch, F. Marin, M. Inguscio, 'Fundamental Noise Source in a High Sensitivity Two Tone Frequency Modulation Spectrometer and Detection of CO_2 at 1.6 μm and 2 μm', *Appl. Phys. B*, **67**, 289 (1998).

127. M.G. Allen, 'Diode-laser Absorption Sensors for Gas-dynamic and Combustion Flows', *Meas. Sci. Technol.*, **9**, 545 (1998).